



A juvenile *Diamantinasaurus matildae* (Dinosauria: Titanosauria) from the Upper Cretaceous Winton Formation of Queensland, Australia, with implications for sauropod ontogeny

Samantha L. Rigby, Stephen F. Poropat, Philip D. Mannion, Adele H. Pentland, Trish Sloan, Steven J. Rumbold, Carlin B. Webster & David A. Elliott

To cite this article: Samantha L. Rigby, Stephen F. Poropat, Philip D. Mannion, Adele H. Pentland, Trish Sloan, Steven J. Rumbold, Carlin B. Webster & David A. Elliott (2022): A juvenile *Diamantinasaurus matildae* (Dinosauria: Titanosauria) from the Upper Cretaceous Winton Formation of Queensland, Australia, with implications for sauropod ontogeny, Journal of Vertebrate Paleontology, DOI: [10.1080/02724634.2021.2047991](https://doi.org/10.1080/02724634.2021.2047991)

To link to this article: <https://doi.org/10.1080/02724634.2021.2047991>



© 2022. Samantha L. Rigby, Stephen F. Poropat, Philip D. Mannion, Adele H. Pentland, Trish Sloan, Steven J. Rumbold, Carlin B. Webster, and David A. Elliott.



[View supplementary material](#)



Published online: 14 Apr 2022.



[Submit your article to this journal](#)



[View related articles](#)



[View Crossmark data](#)

A JUVENILE *DIAMANTINASAUROUS MATILDAE* (DINOSAURIA: TITANOSAURIA) FROM THE UPPER CRETACEOUS WINTON FORMATION OF QUEENSLAND, AUSTRALIA, WITH IMPLICATIONS FOR SAUROPOD ONTOGENY

SAMANTHA L. RIGBY,¹ STEPHEN F. POROPAT,¹ PHILIP D. MANNION,³ ADELE H. PENTLAND,^{1,2} TRISH SLOAN,² STEVEN J. RUMBOLD,² CARLIN B. WEBSTER,² and DAVID A. ELLIOTT²

¹School of Science, Computing and Engineering Technologies, Swinburne University of Technology, John St, Hawthorn, Victoria 3122, Australia, srigby@swin.edu.au; sporopat@swin.edu.au; apentland@swin.edu.au;

²Australian Age of Dinosaurs Museum of Natural History, The Jump-Up, Winton, Queensland 4735, Australia, samantha.rigby@hotmail.com; stephenfporopat@gmail.com; pentlandadele@gmail.com; trish.sloan@aaod.com.au; rumby02@hotmail.com; carlin-webster@hotmail.com; david.elliott@aaod.com.au;

³Department of Earth Sciences, University College London, Gower Street, London WC1E 6BT, U.K., philipdmannion@gmail.com

ABSTRACT—Although sauropod dinosaur bones are the most abundant vertebrate fossils found in the Upper Cretaceous Winton Formation of northeast Australia, only subadult and adult specimens have been described to date. Herein, we describe the first juvenile sauropod from Australia, derived from the Winton Formation (Cenomanian–lower Turonian). The preserved material belongs to a single individual and is sufficiently diagnostic to classify as a juvenile *Diamantinasaurus matildae*—the third specimen to be referred to the species. It also enables the identification of a new local autapomorphy for *Diamantinasaurus*: a distinct tuberosity on the medial surface of the scapula, posterior to the junction of the acromion and the distal blade. Nevertheless, several morphological changes are observable between the juvenile and the two adult skeletons of *Diamantinasaurus matildae*. These include less well-defined or entirely absent muscle attachment sites on the juvenile bones relative to the heavily scarred and rugose adult specimens. Overlapping elements between the juvenile and the two adult skeletons indicate allometric changes for *Diamantinasaurus matildae* throughout ontogeny, with limb bones growing at a more rapid proportional rate than other skeletal elements. Finally, we review the global record of juvenile sauropod remains, demonstrating that the growth patterns of sauropods vary greatly between taxa. Although titanosaurs display a range of isometry and allometry in the growth of individual bones, it appears that allometric growth was the primary pattern for this group.

SUPPLEMENTAL DATA—Supplemental materials are available for this article for free at www.tandfonline.com/UJVP.

Citation for this article: Rigby, S. L., S. F. Poropat, P. D. Mannion, A. H. Pentland, T. Sloan, S. J. Rumbold, C. B. Webster, and D. A. Elliott. 2022. A juvenile *Diamantinasaurus matildae* (Dinosauria: Titanosauria) from the Upper Cretaceous Winton Formation of Queensland, Australia, with implications for sauropod ontogeny. *Journal of Vertebrate Paleontology*. DOI: 10.1080/10.1080/02724634.2021.2047991

INTRODUCTION

Sauropod remains have been discovered in low to mid-paleolatitude Mesozoic strata all over the world (Upchurch et al., 2004). Most sauropod specimens described to date pertain to adult or subadult individuals, with juvenile material less commonly found (Klein and Sander, 2008; Carballido et al., 2012). Juvenile dinosaur remains, especially of herbivorous species, are generally rare in Mesozoic sedimentary deposits worldwide (Varricchio, 2011). Whether this is a consequence of taphonomic

bias in the fossil record towards the preservation of adults, or of collection bias, is unclear, although Hone and Rauhut (2010) suggested that it might be a result of preferential predation on and/or scavenging of juvenile dinosaurs by theropods. The discovery and description of juvenile sauropod individuals is critical for determining their life history and growth strategy (Coria, 1994; Chiappe et al., 1998, 2005; Curry Rogers et al., 2016; Silva Junior et al., 2017; Kundrát et al., 2020). Osteological changes observed between juvenile and adult bones of a given sauropod species might shed light on how these dinosaurs evolved to become the largest land animals to have ever existed (Sander et al., 2004).

To date, no juvenile sauropod material has been reported from Australia, despite sauropods being the most commonly found dinosaurs in the northern half of the continent (Coombes and Molnar, 1981; Molnar and Salisbury, 2005; Hocknull et al., 2009, 2021; Poropat et al., 2015a, 2015b, 2016, 2017, 2020, 2021a, 2021b:table 3). Five sauropod taxa have been established from the Cretaceous Period of Australia: the non-titanosaurian somphospondylan *Austrosaurus mckillopi* from the upper Albian Allaru Mudstone (Longman, 1933); and the non-titanosaurian somphospondylan *Wintonotitan watsi* (Hocknull et al., 2009), and the titanosaurs *Diamantinasaurus matildae* (Hocknull

*Corresponding author

© 2022, Samantha L. Rigby, Stephen F. Poropat, Philip D. Mannion, Adele H. Pentland, Trish Sloan, Steven J. Rumbold, Carlin B. Webster, and David A. Elliott.

This is an Open Access article distributed under the terms of the Creative Commons Attribution-NonCommercial-NoDerivatives License (<http://creativecommons.org/licenses/by-nc-nd/4.0/>), which permits non-commercial re-use, distribution, and reproduction in any medium, provided the original work is properly cited, and is not altered, transformed, or built upon in any way.

Color versions of one or more of the figures in the article can be found online at www.tandfonline.com/ujvp.

et al., 2009), *Savannasaurus elliottorum* (Poropat et al., 2016), and *Australotitan cooperensis* (Hocknull et al., 2021) from the Cenomanian–?lowermost Turonian Winton Formation. The lack of juvenile sauropod material in Australia has heretofore precluded determination of the growth patterns for any of the known taxa on this landmass. Herein, we describe the first juvenile sauropod discovered in Australia, and elucidate the growth pattern strategy of the species to which it is referred. We place this in the broader context of sauropod ontogenetic growth across the clade.

Institutional Abbreviations—**AAOD**, Australian Age of Dinosaurs Museum of Natural History, Winton, Australia; **EMF**, Eromanga Natural History Museum Fossil (Eromanga, Australia); **QM**, Queensland Museum, Brisbane, Australia.

Anatomical Abbreviations—**ACPL**, anterior centroparapophyseal lamina; **CPAF**, centroparapophyseal fossa; **CPOF**, centropostzygapophyseal fossa; **CPOL**, centropostzygapophyseal lamina; **CPRF**, centroprezygapophyseal fossa; **CPRL**, centroprezygapophyseal lamina; **dp**, diapophysis; **PACDF**, parapophyseal centrodiapophyseal fossa; **PACPRF**, parapophyseal centroprezygapophyseal fossa; **PCDL**, posterior centrodiapophyseal lamina; **PCPL**, posterior centroparapophyseal lamina; **POCDF**, postzygapophyseal centrodiapophyseal fossa; **PODL**, postzygodiapophyseal lamina; **POSDF**, postzygapophyseal spinodiapophyseal fossa; **POSL**, postspinal lamina; **poz**, postzygapophysis; **pp**, parapophysis; **PPDL**, parapodiapophyseal lamina; **PRDL**, prezygodiapophyseal lamina; **PRPADE**, prezygapophyseal parapodiapophyseal fossa; **PRPL**, prezygoparapophyseal lamina; **PRSDF**, prezygapophyseal spinodiapophyseal fossa; **PRSL**, prespinal lamina; **prz**, prezygapophysis; **SPDL**, spinodiapophyseal lamina; **SPOF**, spinopostzygapophyseal fossa; **SPOL**, spinopostzygapophyseal lamina; **SPRF**, spinoprezygapophyseal fossa; **SPRL**, spinoprezygapophyseal lamina; **TPOL**, interpostzygapophyseal lamina; **TPRL**, interprezygapophyseal lamina; **vPCPL**, ventral posterior centroparapophyseal lamina.

METHODS

Australian Age of Dinosaurs Locality (AODL) 0122, the ‘Oliver’ site, was excavated with a front-end loader and a small excavator, as well as crowbars, screwdrivers, and geological hammers. Fragile fossil material was consolidated using solutions of 10–25% w/v Paraloid B72 in acetone. The skeletons of AODF 663 (*Diamantinasaurus matildae* individual described herein), AODF 603 (*Diamantinasaurus matildae* holotype individual), AODF 660 (*Savannasaurus elliottorum* holotype individual), AODF 836 (*Diamantinasaurus matildae* referred individual), and AODF 888 (undescribed individual) were surface scanned with an Artec Space Spider handheld laser scanner (www.artec3d.com/portable-3d-scanners/artec-spider-v2), and the resultant three-dimensional models were scaled and manipulated in Artec Studio 15 Professional (www.artec3d.com/3d-software/artec-studio). Figures of three-dimensional models were assembled in Adobe Photoshop 2021 and outlined and annotated in Adobe Illustrator 2021. The terminology used to describe the vertebral laminae and fossae largely follows Wilson (1999) and Wilson et al. (2011), respectively.

To quantitatively assess the nature of ontogenetic growth, we conducted an ordinary least squares regression, using log-transformed measurements of overlapping elements of AODF 663 and AODF 603 (Fig. S1). The measurement taken for the proximal length of the femur of AODF 663 is based on an incomplete specimen. However, we used the femur as the scale against which elements were compared because femoral length in archosaurs, including crocodylians and theropods, is less variable and exhibits a more linear growth than other bones (Currie, 2003; Livingston et al., 2009; Ikejiri, 2015). Following the methods of Currie (2003), the relative size increase of an

element is considered to be isometric when the allometric coefficient (k) is equal to 1.0 (within a 95% confidence interval), with values of $k < 1.0$ and > 1.0 regarded as negative and positive allometry, respectively (Fig. S1).

GEOLOGICAL SETTING

The Winton Formation covers a significant portion of central Queensland and extends into northern New South Wales, north-eastern South Australia, and eastern Northern Territory (Fig. 1) (Cook et al., 2013). It is the youngest Mesozoic stratum in the Eromanga Basin. Age estimates have consistently placed it in the mid Cretaceous (Albian–Cenomanian: Senior et al., 1978; Dettmann et al., 1992) and it has been informally subdivided into ‘lower’ and ‘upper’ members, with exposures around Winton placed in the ‘upper’ Winton Formation and regarded as Cenomanian–? lowermost Turonian (Tucker et al., 2017). It is interpreted to have been deposited within an extensive, forested floodplain that formed during and after the recession of the Eromanga Sea (Cook et al., 2013; Tucker et al., 2013, 2017; Fletcher et al., 2018). At the beginning of the Late Cretaceous, the Winton area would have been situated at approximately 50°S (Van Hinsbergen et al., 2015) and had a warm and temperate climate, with annual mean average temperatures of 15–16° based on various analyses of fossil leaves and wood (Fletcher et al., 2013, 2014, 2015).

AODL 0122 is located on Elderslie Station, approximately 60 km west-northwest of Winton, Queensland, Australia. The site was discovered by the owners of the property, who identified fragments of the right femur and dorsal ribs at the surface. These fragments were heavily eroded and found in the weathered soil layer, commonly referred to as ‘black soil,’ as is common in Winton Formation deposits. Excavations at the site revealed the less-weathered siltstones of the Winton Formation below. Some elements, notably several dorsal ribs and the femur, were present at the transition between the ‘black soil’ and the siltstone, whereas the majority of the remaining bones were present exclusively within the siltstone.

The blue-gray to pale gray siltstone layer in which this specimen was found was relatively thin and pinched out at the margins of the main bone concentration. The only non-sauropod fossil recovered from the siltstone layer was an indeterminate bivalve. Immediately beneath the bone-bearing layer, a much paler, fine sandstone was present, containing abundant angiosperm, ginkgo, and fern leaves.

Although the remains of AODF 663 were disarticulated when discovered (Fig. S2), two dorsal centra were found in contact with one another, along with one of the dorsal ribs. A cluster of four ribs from the right-hand side of the body were also recovered together. Given that all elements were discovered in close proximity to each other, are size congruent, and show no duplication, we interpret all elements from this site to represent a single sauropod individual.

SYSTEMATIC PALEONTOLOGY

SAUROPODA Marsh, 1878

MACRONARIA Wilson and Sereno, 1998

TITANOSAURIFORMES Salgado, Coria and Calvo, 1997

SOMPHOSPONDYLI Wilson and Sereno, 1998

TITANOSAURIA Bonaparte and Coria, 1993

DIAMANTINASAURIA Poropat, Kundrát, Mannion, Upchurch, Tischler and Elliott, 2021a

DIAMANTINASAURUS MATILDAE Hocknull, White, Tischler, Cook, Calleja, Sloan and Elliott, 2009

Holotype Specimen—AODF 603: partial postcranial skeleton including three partial cervical ribs, three incomplete dorsal vertebrae*, dorsal ribs, fragmentary gastralia, five coalesced sacral vertebrae*, isolated sacral processes, left* and right scapulae,

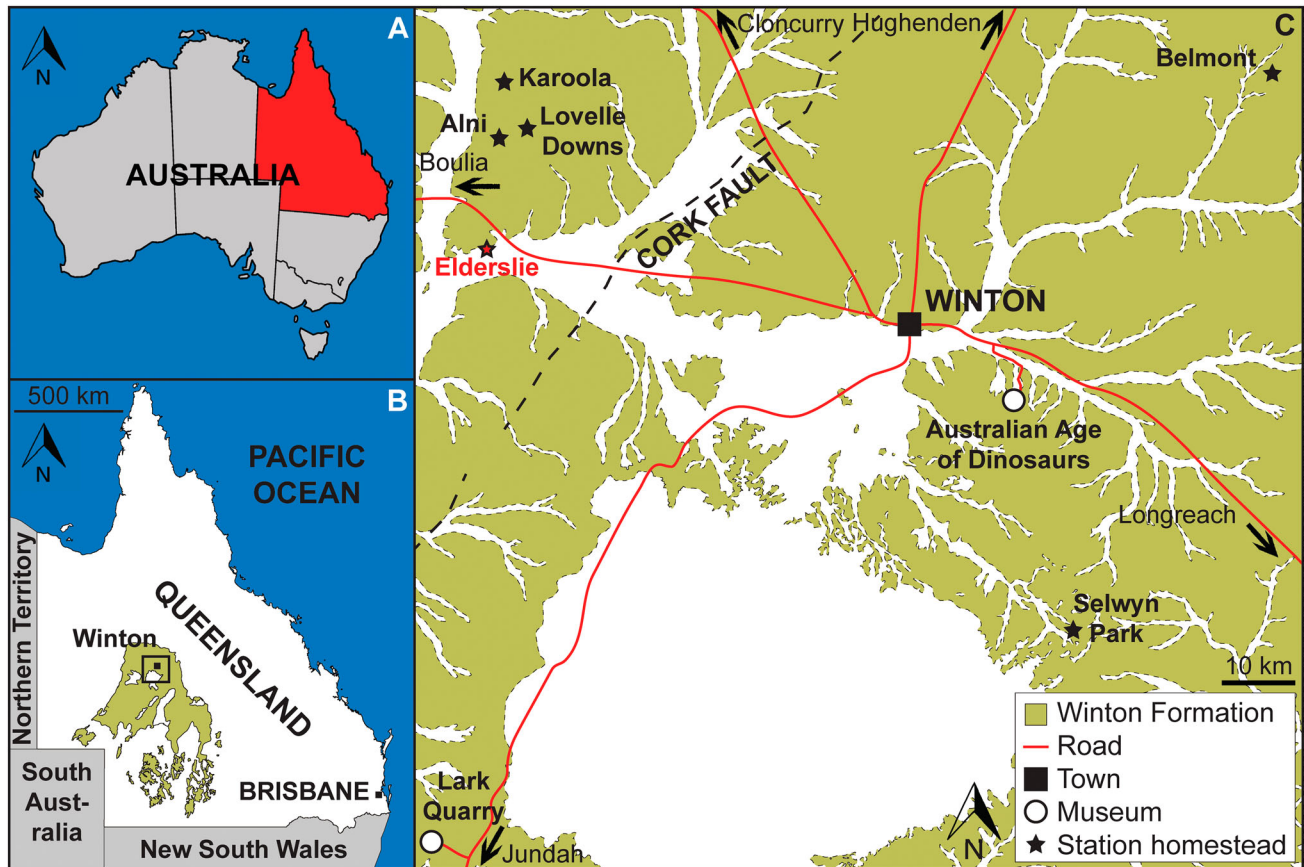


FIGURE 1. Map of Queensland, Australia showing the location of Winton, with an inset of the locations of the various sheep stations (including Elderslie, from which AODF 663 was recovered) on which sauropod remains have been discovered, and the Dinosaur Stampede National Monument at Lark Quarry Conservation Park (modified from Poropat et al., 2021a).

right coracoid*, sternal plate*, left and right humeri, left* and right ulnae, right radius*, left and right* metacarpals I–V, eight manual phalanges (including manual ungual I-2), left ilium, left and right pubes, left and right ischia, right femur, right tibia, right fibula, right astragalus [Elements from the same individual formerly regarded as paratypes marked with an asterisk] (Hocknull et al., 2009; Poropat et al., 2015b).

Previously Referred Specimen—AODF 836: partial skull with associated postcranial skeleton including cervical and dorsal vertebrae; cervical and dorsal ribs; partial scapula; left and right iliac preacetabular processes; paired pubes; left and right ischia (Poropat et al., 2016, 2021a).

Newly Referred Specimen—AODF 663 (‘Oliver’): one cervical rib; two dorsal vertebral centra; three dorsal neural arches; several dorsal ribs; left scapula; right humerus; right manual phalanx I-2; right femur; associated fragments.

Locality—AODL 0122 (the ‘Oliver’ site), Elderslie Station, ca. 60 km west-northwest of Winton, Queensland, Australia.

Horizon and Age—Upper Winton Formation, lower Upper Cretaceous (Cenomanian–?lowermost Turonian).

Revised Diagnosis—To the diagnosis of *Diamantinasaurus matildae* presented by Poropat et al. (2021a), we append one local autapomorphy: scapula medial surface with distinct tuberosity just posterior to the junction of the acromion and the distal blade (also identified by Hocknull et al., 2021).

DESCRIPTION AND COMPARISONS

AODF 663 clearly represents a juvenile individual (*sensu* Hone et al., 2016; Griffin et al., 2021): the neurocentral sutures on the dorsal vertebrae are unfused; the cortex of the femur is open; the bones lack rugose texturing; and the elements are far smaller than most known sauropod individuals (proximodistal length of the right humerus of AODF 663 is 698 mm, whereas it is 1068 mm for the right humerus of AODF 603 [adult *Diamantinasaurus* holotype]).

The AODF 663 specimen overlaps anatomically with the holotype specimens of each of the four named sauropods from the Winton Formation: *Wintonotitan watsi* (Hocknull et al., 2009; Poropat et al., 2015a), *Diamantinasaurus matildae* (Hocknull et al., 2009; Poropat et al., 2015b), *Savannasaurus elliotorum* (Poropat et al., 2016, 2020), and *Australotitan cooperensis* (Hocknull et al., 2021), as well as a previously referred specimen (AODF 836) of *D. matildae* (Poropat et al., 2016, 2021a) (Table 1). Poropat et al. (2021a) recently established the clade Diamantinasauria, comprising *Diamantinasaurus* and *Savannasaurus*, as well as *Sarmientosaurus musacchioi*, from Argentina, although the latter species does not overlap anatomically with AODF 663 (Martínez et al., 2016). Hocknull et al. (2021) further supported this clade, resolving *Australotitan* and *Wintonotitan* within Diamantinasauria.

TABLE 1. Material of AODF 663 as preserved in named Winton Formation specimens. *Indicates an incompletely preserved element.

Element	<i>Diamantinasaurus matildae</i> AODF 663	<i>Diamantinasaurus matildae</i> AODF 603	<i>Diamantinasaurus matildae</i> AODF 836	<i>Savannasaurus elliottorum</i> AODF 660	<i>Wintonotitan watsi</i> QM F7292	<i>Australotitan cooperensis</i> EMF102
Cervical ribs	Left × 1	Left* and Right*	Right × 1	Left × 4	No	No
Dorsal vertebrae	I–III	III, X	4 total including VI and VII	III–X	Several fragmentary	No
Dorsal ribs	Yes	Yes	Yes	Yes	Yes*	No
Scapula	Left	Left* and Right*	Right*	-	Left*	Left*
Humerus	Right	Left and Right	-	Left* and Right*	Left* and Right*	Left* and Right
Manual ungual I-2	Left	Left	-	-	-	No
Femur	Right	Right	-	-	-	Left* and Right*

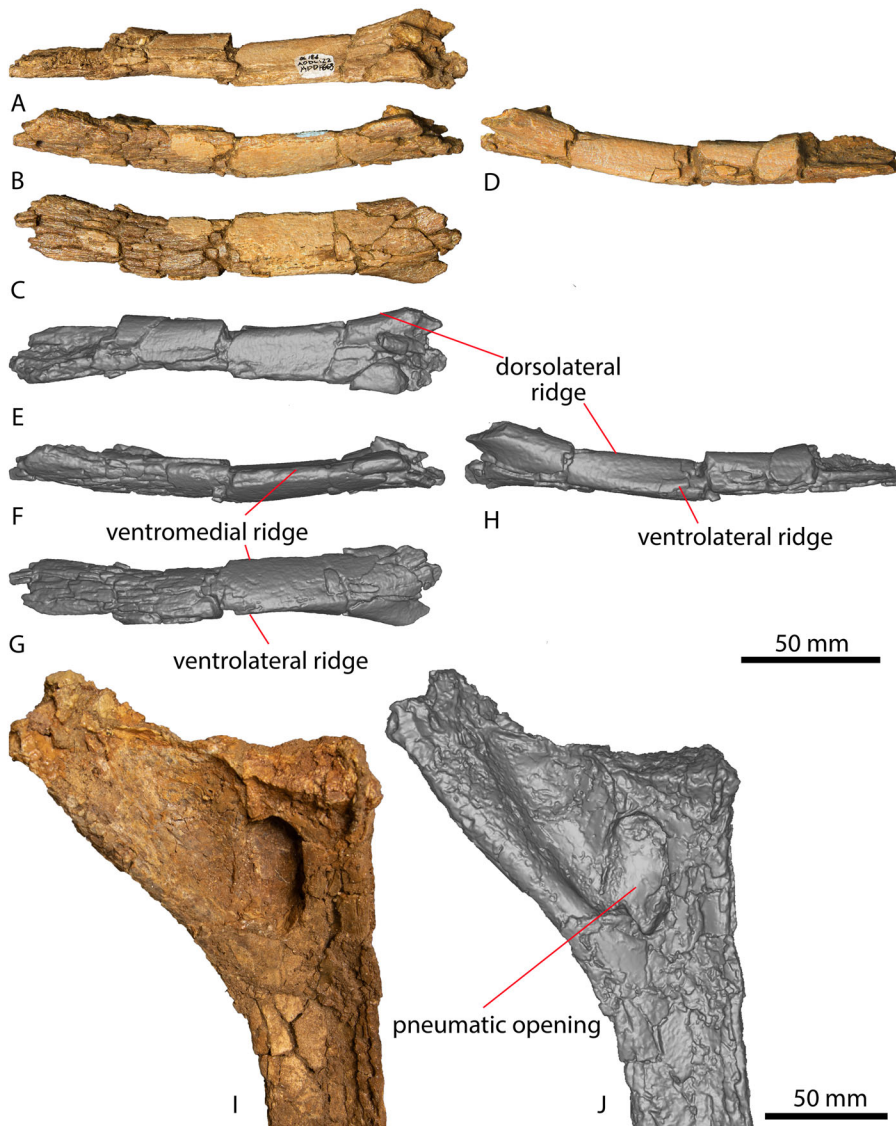


FIGURE 2. AODF 663 left cervical rib and dorsal rib. Left cervical rib photographs in **A**, dorsal, **B**, medial, **C**, ventral, **D**, lateral views. Left cervical rib digital models in **E**, dorsal, **F**, medial, **G**, ventral, **H**, lateral views. Dorsal rib photograph in **I**, posterior view. Dorsal rib digital model in **J**, posterior view.

Cervical Rib

One partial left cervical rib is preserved in AODF 663 (Fig. 2). Both ends are incomplete, with the distal end slightly distorted as

a result of infiltration by ‘black soil.’ It is tentatively identified as an anterior cervical rib, owing to its small size and similarity to the right anterior cervical rib of AODF 836 (Fig. 3) (Poropat et al., 2021a; note that this was mistakenly identified as a left

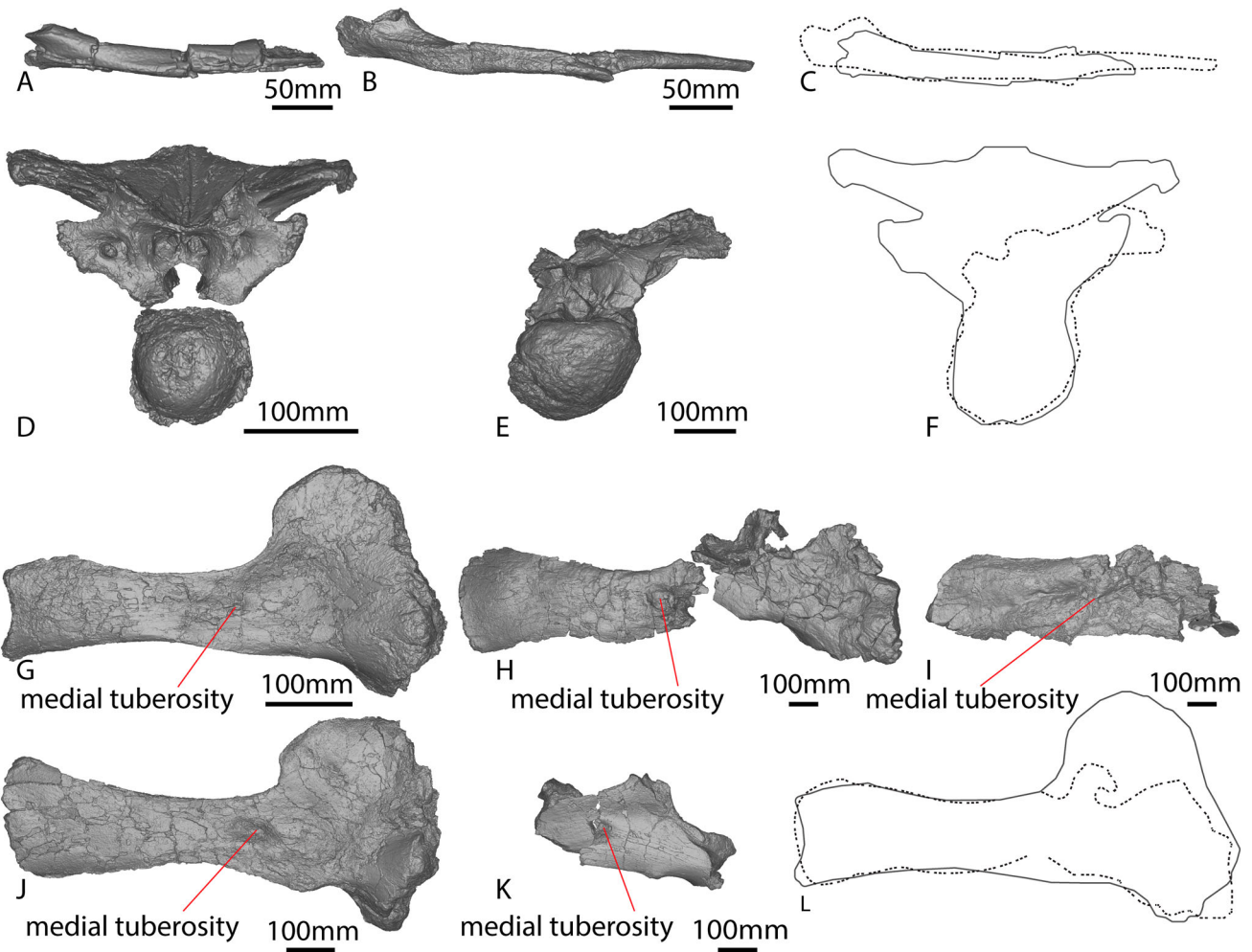


FIGURE 3. Comparisons between axial elements and scapulae. AODF 663 left cervical rib in **A**, anterior. AODF 836 right cervical rib mirrored in **B**, anterior. AODF 663 (solid line) and AODF 836 (dotted line) cervical rib outlines **C**, overlaid to the same size. AODF 663 dorsal vertebra B in **D**, anterior. AODF 603 dorsal vertebra B in **E**, anterior. AODF 663 (solid line) and AODF 603 (dotted line) dorsal vertebra outlines **F**, overlaid to the same size. AODF 663 left scapula in **G**, posterior. AODF 603 left scapula in **H**, posterior. AODF 603 right scapula mirrored in **I**, posterior. AODF 888 left scapula in **J**, posterior. AODF 836 right scapula mirrored in **K**, posterior. AODF 663 (solid line) and AODF 603 (dotted line) scapula outlines **L**, overlaid to the same size.

element in the caption of fig. 23 in Poropat et al. [2021a]). A dorso-lateral ridge runs proximodistally along the preserved length of the cervical rib. This is situated close to the lateral margin at the proximal end, migrating dorsally towards the distal end, and has previously been identified as an autapomorphy of *Diamantinasaurus* (Poropat et al., 2015b, 2021a). Subtle ridges define the ventromedial and ventrolateral margins of the rib, as also observed in *Diamantinasaurus* (Poropat et al., 2015b, 2021a). Owing to the incompleteness of the rib, the proximodistal extent of these ridges cannot be determined. The only preserved cervical ribs in *Savannasaurus* lack the aforementioned ridges, although these ribs derive from further back in the cervical series, rendering comparison with AODF 663 less meaningful.

Dorsal Vertebrae

AODF 663 preserves three partial dorsal neural arches and two dorsal centra (Figs. 4–6). Two of the centra appear to belong with two of the neural arches, meaning a minimum of three vertebrae are represented; herein, these are designated dorsal vertebrae A, B, and C. The internal tissue structure of

all preserved vertebrae is camellate, as is the case in all titanosauriforms (Wedel, 2003).

All that remains of dorsal vertebra A is an incomplete neural arch, preserving the neural canal, the bases of the parapophyses, and the lower sections of several laminae (Fig. 4). This neural arch is anteroposteriorly shorter than either of the other neural arches recovered. Based on the position of the parapophysis at the level of the neurocentral suture, we suggest that this vertebra was closer to the base of the neck than dorsal vertebrae B or C, and tentatively interpret it as dorsal vertebra II following comparisons with Australian sauropod specimens with more complete vertebral series (Poropat et al., 2016, 2017, 2020).

The centrum and neural arch of dorsal vertebra B (Fig. 5) were found in close association, albeit rotated 90° relative to one another. These elements clearly fit together but were not fused in life, indicating that AODF 663 never reached osteological maturity. The centrum was found in contact with the proximal end of a left dorsal rib and in association with other axial skeletal remains, attesting to relatively little post mortem disturbance that facilitated almost complete preservation of the vertebra. Based on the natural dorsoventral compression of

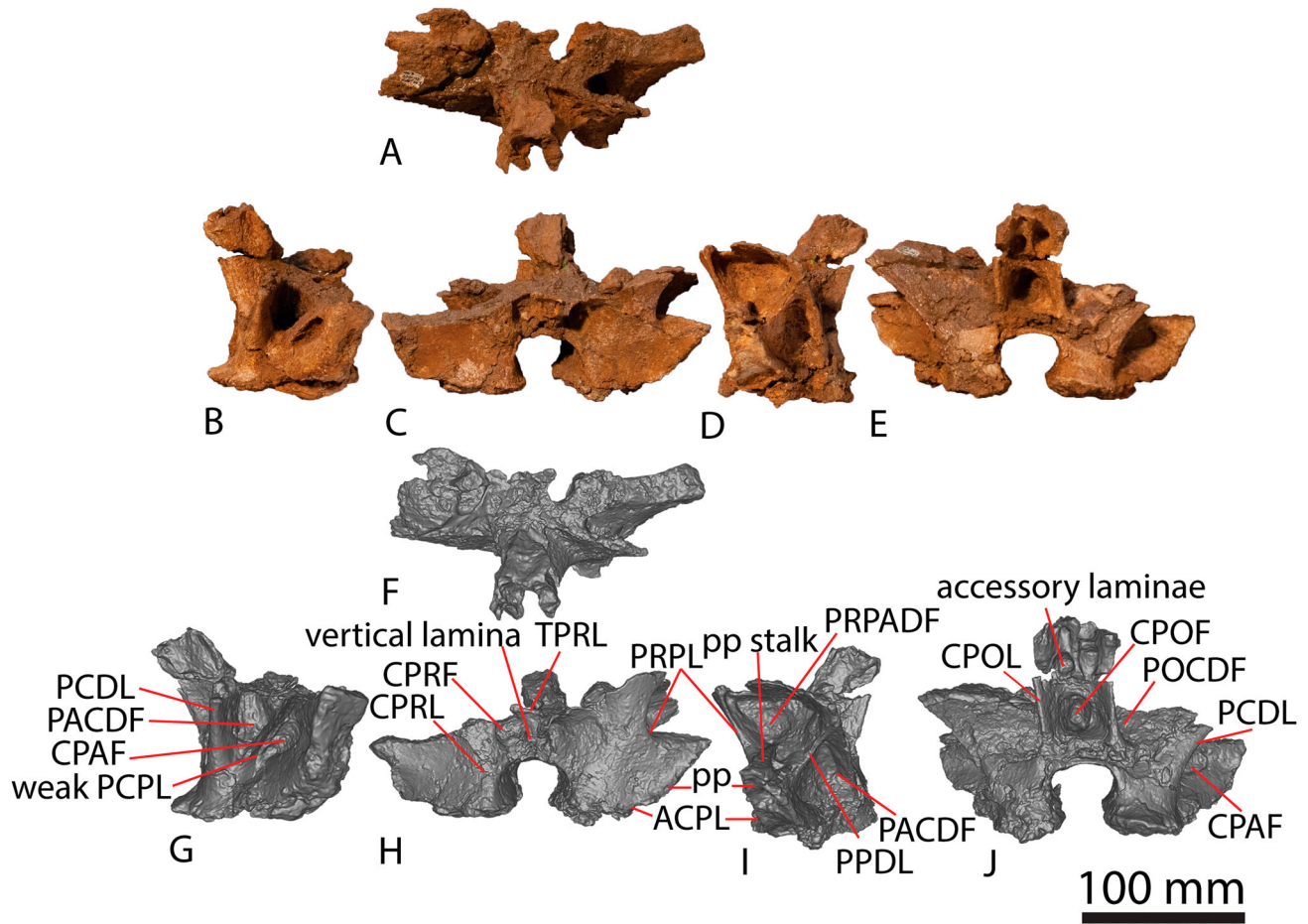


FIGURE 4. AODF 663 dorsal vertebra A. Dorsal vertebra A photographs in **A**, dorsal, **B**, right lateral, **C**, anterior, **D**, left lateral, **E**, posterior views. Dorsal vertebra A digital models in **F**, dorsal, **G**, right lateral, **H**, anterior, **I**, left lateral, **J**, posterior views.

the centrum, the relative positions of the parapophyses and diapophyses (both located entirely on the neural arch, with each parapophysis situated anteroventral to the diapophysis), the wide spacing of the prezygapophyses, and the posterodorsal orientation of the neural spine, we tentatively interpret this as dorsal vertebra III.

Both the centrum and the neural arch of dorsal vertebra C are preserved (Fig. 6). The neural arch was recovered in several pieces and can only be tentatively reconstructed. The left half of the neural arch is much more complete than the right, although both are morphologically similar and closely resemble the morphology of the neural arch of dorsal vertebra B. The parapophysis of dorsal vertebra C is situated further up the neural arch than in dorsal vertebra B (although still not at the level of the prezygapophysis), indicating that this vertebra was located more posteriorly than dorsal vertebra B. Based on the relative anteroposterior length of this element, the larger anterior condyle and posterior cotyle, the greater size of the lateral pneumatic fossa and foramen (Table S1), and the position of the parapophysis, we interpret this vertebra as the posteriormost preserved in AODF 663, most likely dorsal vertebra IV.

Each centrum is opisthocoelous, and the anterior and posterior articular surfaces are shorter dorsoventrally than they are wide transversely. The articular surfaces resemble the middle–posterior dorsal vertebrae of *Diamantinasaurus* (Figs. 3D–F) (Poropat et al., 2015b, 2021a) and are less dorsoventrally

compressed than in dorsal vertebrae III–VII of *Savannasaurus* (Poropat et al., 2020). The depth of concavity of the posterior cotyle is similar to that of *Diamantinasaurus*, but contrasts with *Wintonotitan* and *Savannasaurus*, which have deeper and shallower cotyles, respectively, although this might be reflective of the serial position of the vertebrae or an ontogenetic overprint. All centra appear to lack the ventral midline keel and fossae that characterize the middle–posterior dorsal vertebrae of *Diamantinasaurus* (Poropat et al., 2015b), and the ridges observed in the anterior dorsal vertebrae of *Austrosaurus* (Poropat et al., 2017). Midline ventral keels are not present on any of the dorsal vertebrae of *Savannasaurus* (Poropat et al., 2020). The ventral surfaces of the AODF 663 centra are anteroposteriorly concave and transversely convex, largely as a result of the expansion of the articular ends; this contrasts with the transversely concave ventral surfaces of the dorsal vertebrae of *Diamantinasaurus* (Poropat et al., 2015b, 2021a) and *Savannasaurus* (Poropat et al., 2020). The lateral surfaces of each centrum host a pneumatic foramen, clearly set within a subtly defined fossa. In dorsal vertebra B, this foramen is less than half the length of the centrum overall, and it is strongly anteriorly biased. The pneumatic foramen in dorsal vertebra C is more anteroposteriorly elongate and posteriorly acuminate, as in *Diamantinasaurus* (Poropat et al., 2015b). By contrast, the pneumatic foramina of the dorsal vertebrae *Savannasaurus* are relatively smaller than AODF 663. The dorsal margin of each centrum of AODF 663 is characterized by a raised, laterally projecting lip, representing

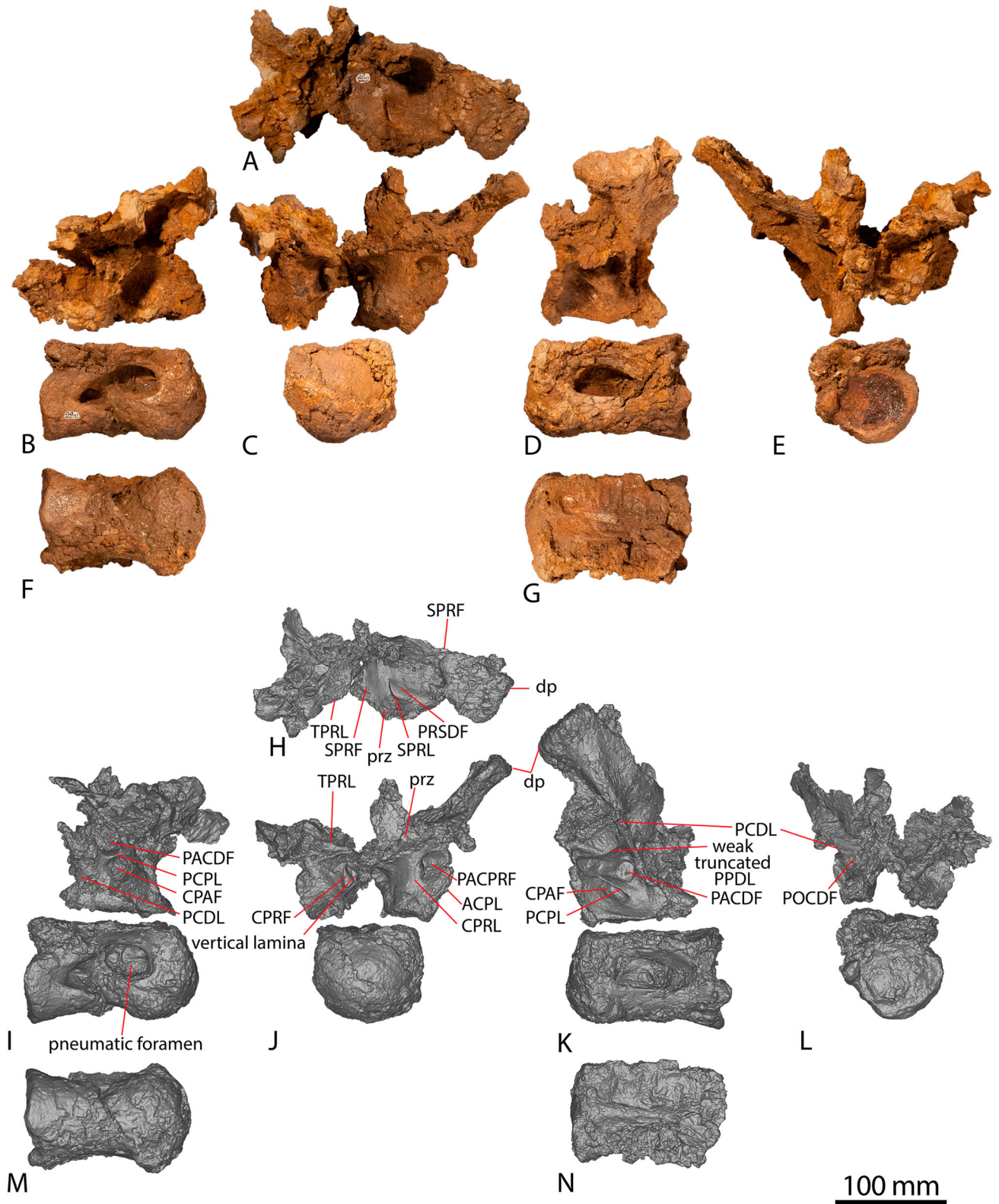


FIGURE 6. AODF 663 dorsal vertebra C. Dorsal vertebra C photographs in **A**, dorsal, **B**, right lateral, **C**, anterior, **D**, left lateral, **E**, posterior, **F**, ventral, **G**, centrum dorsal views. Dorsal vertebra C digital models in **H**, dorsal, **I**, right lateral, **J**, anterior, **K**, left lateral, **L**, posterior, **M**, ventral, **N**, centrum dorsal views.

the point of contact with the neural arch; this would have been obliterated had the neurocentral suture fused.

The most complete dorsal neural arch in AODF 663 is dorsal vertebra B; thus, unless otherwise stated, the following description is primarily based on this specimen. Each prezygapophyseal articular facet is slightly shorter anteroposteriorly (37 mm) than it is wide mediolaterally (40 mm). Each prezygapophysis is supported from below by a single CPRL; this contrasts with the excavated CPRLs in the dorsal vertebrae of *Savannasaurus*, with medial and lateral branches forming, at least on the left side (Poropat et al., 2020). In AODF 663, the CPRL, the anterior ACPL, and the PRPL define a triangular PACPRF on the anterior surface of the neural arch. This fossa is situated more medially than in *Savannasaurus*. The prezygapophyses are connected to one another on their medial surfaces by a TPRL, which forms the dorsal margin of the CPRF, bounded laterally by the CPRL. This might vary serially, as is the case for the TPRLs of *Diamantinasaurus* and *Savannasaurus*, wherein the TPRLs form the roof of the neural canal of posterior dorsal vertebrae (Poropat et al., 2015b, 2020). The CPRF is bisected by a thin, vertical lamina that extends from the TPRL to the dorsal margin of the anterior neural canal opening, as in the anterior and middle dorsal vertebrae of *Diamantinasaurus* (Poropat et al., 2015b, 2021a) and *Savannasaurus* (Poropat et al., 2020). The base of the anterior surface of the neural arch is smooth and mediolaterally convex either side of the neural canal opening in dorsal vertebrae A and C, but flat in dorsal vertebra B.

The parapophysis of dorsal vertebra A is situated just dorsal to the neurocentral suture and is better preserved on the left side. The parapophyseal articular facets of dorsal vertebra B are significantly taller dorsoventrally (45 mm) than they are long anteroposteriorly (20 mm). The maximum transverse breadth across the paired parapophyses is 207 mm, significantly less than that across the diapophyses (334 mm; Table S1). On each side, the parapophysis is connected to the centrum by a sub-vertical ACPL. On the right side, a weak, anterodorsally–posteroventrally inclined PCPL is also present, with a CPAF present between it and the ACPL. Unlike in *Diamantinasaurus*, the PCPL does not appear to bifurcate anteriorly; although this was provisionally posited as an autapomorphic feature of *Diamantinasaurus* by Poropat et al. (2015b), this was only recognized on a vertebra situated more posteriorly than those preserved in AODF 663. There is no PCPL, and therefore no CPAF, on the left side of dorsal vertebra B. The parapophysis is connected to the prezygapophysis via a well-defined PRPL. On the right side of dorsal vertebra A, there is a second, less-developed lamina that runs parallel to the PRPL; this is absent on the left side. As preserved in dorsal vertebra C, it appears that an accessory lamina is present between the parapophysis and the diapophysis, ventral to the position that would have been occupied by the true PPDL if it were present. Although it is possible that this surface has been damaged, the fact that this lamina can be observed on both sides of the neural arch suggests that it is a genuine feature.

The right diapophysis of dorsal vertebra B is the more completely preserved of the paired diapophyses, although little of the left process is missing. The right diapophysis is twice as long anteroposteriorly as it is tall dorsoventrally. The diapophysis is braced by several robust laminae: ventrally by an anterodorsally–posteroventrally inclined PCDL; posteriorly by a posteromedially–anterolaterally oriented SPDL; and anteriorly by an anteromedially–posterolaterally inclined PRDL. These laminae are similarly robust in *Savannasaurus* (Poropat et al., 2020). In dorsal vertebra B, the left PCDL is not bifurcated ventrally, as in *Diamantinasaurus* and *Savannasaurus* (Poropat et al., 2015b, 2020), and is instead ventrally supported by an additional posterodorsally–anteroventrally angled lamina that appears to represent the PPDL. By contrast, the right PCDL is braced ventrally by two laminae that emerge from the parapophysis. The more

dorsal of these runs from the posterodorsal margin of the parapophysis, whereas the more ventral one runs from the posteroventral margin; thus, both represent PPDLs. A single PPDL is present only on the left side of dorsal vertebra A. The presence or absence of a fully developed PPDL in dorsal vertebra C cannot be established because of the incomplete preservation of the parapophysis, although the anterior margin of the diapophysis is indicative of some connection between the two processes. A PRPADF is present on both sides of the neural arch and bordered in each case by the PRPL, PRDL, and PPDL (upper PPDL on the right side). The PPDL (lower PPDL on the right side), PCPL, and PCDL define a PACDF. The CPAF and PACDF are deep, as in *Savannasaurus* (Poropat et al., 2020).

The postzygapophyses are closely spaced and descend from the posteroventral surface of the neural spine. The articular facet of each postzygapophysis faces ventrolaterally. The dorso-lateral margin of the facet is connected to the posterior surface of the neural spine via a stout, short SPOL. A weakly defined lamina extends from the ventral margin of the postzygapophyseal articular facet towards the diapophysis, terminating at the mid-length of the SPDL; this appears to represent an anteriorly truncated, incipient PODL. The triangular POSDF is bordered by the PODL ventrally, the SPDL dorsally, and the SPOL posteriorly. The PODL separates the POSDF from the much larger POCDF, which is bordered by the PCDL anteroventrally, the SPDL (and PODL) dorsally, and the CPOL posteriorly. A PODL is absent in dorsal vertebra III of *Savannasaurus*, thereby making the POCDF confluent with the POSDF (Poropat et al., 2020). The ventromedial margin of the postzygapophyseal articular facet is supported ventrally by a strongly defined CPOL, which is located close to the midline. Indeed, the lateral margins of the paired CPOLs are only 30 mm apart, and they are in line with the lateral margins of the posterior neural canal opening. This contrasts with *Savannasaurus*, wherein the CPOLs project further ventrally to define the lateral margins of the neural canal (Poropat et al., 2020). The paired CPOLs and the dorsal margin of the posterior neural canal opening form a deep CPOF that is confluent with the SPOF, in the absence of a TPOL and the lack of midline contact between the postzygapophyses. By contrast, in dorsal vertebra III of *Savannasaurus*, a TPOL is present and forms the dorsal margin of the CPOF (Poropat et al., 2020). The POSL extends along the entire preserved posterior surface of the neural spine. Dorsal to the near-junction of the postzygapophyses, the lateral surfaces of the POSL and the medial surfaces of the SPOLs form relatively deep SPOFs, unlike *Wintonotitan*, wherein SPOFs are either shallow or absent (Poropat et al., 2015a). Accessory horizontal laminae brace the POSL within these concavities, as seen in at least one dorsal neural arch of *Wintonotitan* (Poropat et al., 2015a).

The anterior surface of dorsal neural spine A is incomplete, but it appears to preserve a faint PRSL and a fragment of the right SPRL. The neural spine of dorsal vertebra B is angled at 50° relative to the ventral surface of the neural arch. Although it is not well preserved, it seems that the neural spine of dorsal vertebra C was more or less horizontal, such that the SPRL is present but only prominent near the prezygapophysis. A transversely narrow, yet well-defined PRSL is present along almost the entire length of the neural spine of dorsal vertebra B, terminating just posterior to the posterior margins of the prezygapophyses; this is unlike the weakly developed PRSL of *Wintonotitan* (Poropat et al., 2015a). The PRSL is not bifurcated ventrally and does not extend as far anteroventrally to intersect with the TPRLs, as in *Diamantinasaurus* (Poropat et al., 2015b). Rather, it terminates just posterior to the prezygapophyseal articular facets, as in *Savannasaurus* (Poropat et al., 2020). The PRSL is flanked on either side by a weakly developed SPRL that extends from the posteromedial margin of the

prezygapophyseal articular facet to about the mid-height of the neural spine. The SPRLs are not as pronounced as in *Diamantinasaurus*, nor do they extend as far dorsally along the neural spine, (Poropat et al., 2015b). Furthermore, the deep PRSDF found in *Diamantinasaurus* and (to a lesser extent) *Savannasaurus*, is absent in AODF 663. The SPRL defines the lateral margin of the SPRF and does not extend as far dorsally along the neural spine as in *Wintonotitan*. As described above, the posterior surface hosts a POSL and paired SPOLs (supporting the postzygapophyses), whereas the lateral margins of the neural spine are formed by anterolaterally flaring SPDLs. Owing to the fact that the apex of the neural spine is not preserved, it is not possible to determine whether or not aliform processes were present, nor if the neural spine is bifurcated. Additionally, the concavity and rounded median ridge linking the PRSL and POSL—an autapomorphic feature of *Wintonotitan* (Poropat et al., 2015a)—appears to be absent on AODL 663, although this could be attributable to non-preservation rather than genuine absence.

Dorsal Ribs

A total of nine partial dorsal ribs were recovered from AODF 663: two from the left side, four from the right, and three of indeterminate position. The proximal ends preserve evidence of pneumatization, particularly on the posterior surface (Fig. 2I, J). The distal ends of most elements are plank-like in cross section, as in all titanosauriforms (Wilson and Sereno, 1998; Wilson, 2002).

Scapula

The essentially complete left scapula of AODF 663 (Fig. 7) is well-preserved, appears to have experienced very little (if any) post mortem distortion, and is missing only a small portion of bone at each of the proximal and distal ends (the latter was damaged during excavation). The scapula is described with the long axis of the distal blade oriented horizontally.

The scapula can be broadly divided into a ventrally-tapering, ovate acromion and a rectangular distal blade. With the longitudinal axis of the blade oriented horizontally, the coracoid articulation is angled at 70° relative to the horizontal. This is similar to *Diamantinasaurus* (see Fig. 3H for an updated reconstruction of the angle of this element), but differs from the near-perpendicular angle in *Australotitan*, as reconstructed by Hocknull et al. (2021). The wedge-shaped coracoid articular surface is essentially straight, unlike the undulating surface seen in several other macronarians, such as the early-branching *Tehuelchesaurus* (Carballido et al., 2011), and the somphospondylans *Euhelopus* (Young, 1935) and *Daxiatitan* (You et al., 2008). This surface is significantly longer dorsoventrally than the glenoid fossa, but is mediolaterally narrower (Table S1). The glenoid is slightly bevelled medially (Fig. 7G), as is the case in nearly all somphospondylans (Wilson, 2002), but contrasting with the laterally deflected glenoid of the two adult specimens of *Diamantinasaurus* (Poropat et al., 2015b, 2021). The medial margin of the glenoid region is essentially straight in AODF 663, whereas the lateral margin is dorsoventrally convex; consequently, the glenoid is more or less wedge-shaped. Just ventral to the junction between the glenoid and the coracoid articulation, the glenoid reaches its greatest mediolateral width.

The lateral surface of the anterodorsal portion of the acromion is shallowly concave, distinguishing it from *Wintonotitan* (Poropat et al., 2015a). This depression extends to both the dorsal and anterior margins, whereas it is bounded posteriorly–posterovertrally by the acromial ridge, and ventrally by the ventral buttress. The anteroposteriorly convex acromial ridge is

prominent and runs essentially dorsoventrally along most of its length. At its ventral-most point it changes direction, such that it is directed anterovertrally. The angle of the acromial ridge differs from *Wintonotitan* (Poropat et al., 2015a) and shares some resemblance with *Australotitan* (Hocknull et al., 2021), but the non-preservation of this scapular portion in *Diamantinasaurus* (Poropat et al., 2015b, 2021a) precludes further comparisons. A subtly expressed concave region is present immediately posterior to the acromion ridge. The remainder of the lateral surface of the acromion, i.e., the glenoid region, is shallowly anteroposteriorly convex to flat. The medial surface of the acromion is dorsoventrally convex.

At the ventral margin of the acromion, a mediolaterally thickened, but posteriorly diminishing, ridge is present. This ventral buttress extends from the junction between the coracoid articulation and glenoid fossa until slightly beyond the level of the posterior margin of the acromion. This portion of the scapula is not adequately represented in any of the named Winton Formation sauropod species. There is no distinct process on the ventral margin of the scapula, differing from the condition in many eusauropods (Carballido et al., 2011; Mannion et al., 2013), including *Diamantinasaurus* and *Wintonotitan* (Hocknull et al., 2009; Poropat et al., 2015a, 2015b), in which such a process is present on the posterior portion of the acromion.

The proximal portion of the scapular blade is ‘D’-shaped to crescent-shaped in cross section, as in *Diamantinasaurus* (Poropat et al., 2015b; Hocknull et al., 2021) and most eusauropods (Wilson, 2002; Carballido et al., 2020), but differing from the flattened cross section that characterizes *Wintonotitan* (Hocknull et al., 2009; Poropat et al., 2015a). The blade maintains a relatively consistent dorsoventral height along its length, although it does slightly expand dorsoventrally towards the distal end, as in *Diamantinasaurus* (Poropat et al., 2015b). The lateral surface of the blade is weakly anteroposteriorly convex and distinctly bowed laterally, resulting in this surface being strongly dorsoventrally convex. This contrasts with the scapula of *Australotitan* (Hocknull et al., 2021); however, this element has suffered major taphonomic distortion, limiting meaningful comparison with AODF 663. Towards the distal end, the blade becomes flatter dorsoventrally, unlike *Diamantinasaurus* and *Wintonotitan* (Poropat et al., 2015a, 2015b). The lateral surface lacks an accessory longitudinal ridge and fossa, which was identified as an autapomorphy of *Diamantinasaurus* by Poropat et al. (2015b).

Virtually the entire medial surface of the scapular blade is anteroposteriorly concave, other than a low tuberosity just posterior to the junction of the acromion process and the scapular blade, situated approximately at midheight. This tuberosity is also present in the two adult *Diamantinasaurus* specimens (AODF 603 and AODF 836), the holotype specimen of *Wintonotitan wattsi* (Hocknull et al., 2021), and an as yet undescribed sauropod specimen from the Winton Formation (AODF 888) (see Fig. 3G–K). This tuberosity was interpreted to be absent in *Australotitan* and was proposed to be a shared characteristic between *Diamantinasaurus* and *Wintonotitan* by Hocknull et al. (2021). However, closer inspection of *Australotitan* suggests that the relevant region of the scapula is not well enough preserved to confirm its absence. There is a possibility that the tuberosity is partially preserved at the ventral-most portion of the scapula in that taxon (see Hocknull et al., 2021:fig. 9B). The tuberosity is located closer to the dorsal margin in *Wintonotitan*, in which it is also proximodistally expanded, whereas in *Diamantinasaurus* it is located at the midline as a slight bulge. Although a medial tuberosity or ridge is present on the proximal portion of the scapular blade of several titanosaurs (Sanz et al., 1999; Upchurch et al., 2004), this is situated close to the dorsal margin. By contrast, a small number of diplodocoids are



FIGURE 7. AODF 663 left scapula. Left scapula photographs in **A**, dorsal, **B**, posterior, **C**, medial, **D**, anterior, **E**, ventral views. Left scapula digital models in **F**, dorsal, **G**, posterior, **H**, medial, **I**, anterior, and **J**, ventral views.

characterized by a tuberosity at midheight (Whitlock, 2011; Tschopp et al., 2015), with this prominently developed in the rebbachisaurid *Nigersaurus* (Serenó et al., 1999). This feature therefore represents a newly recognized local autapomorphy of

Diamantinasaurus matildae. No dorsal or ventral ridges are present on the medial surface of the blade. The deep fossa present at the junction between the acromion and scapular blade observed in *Wintonotitan*, and interpreted as an

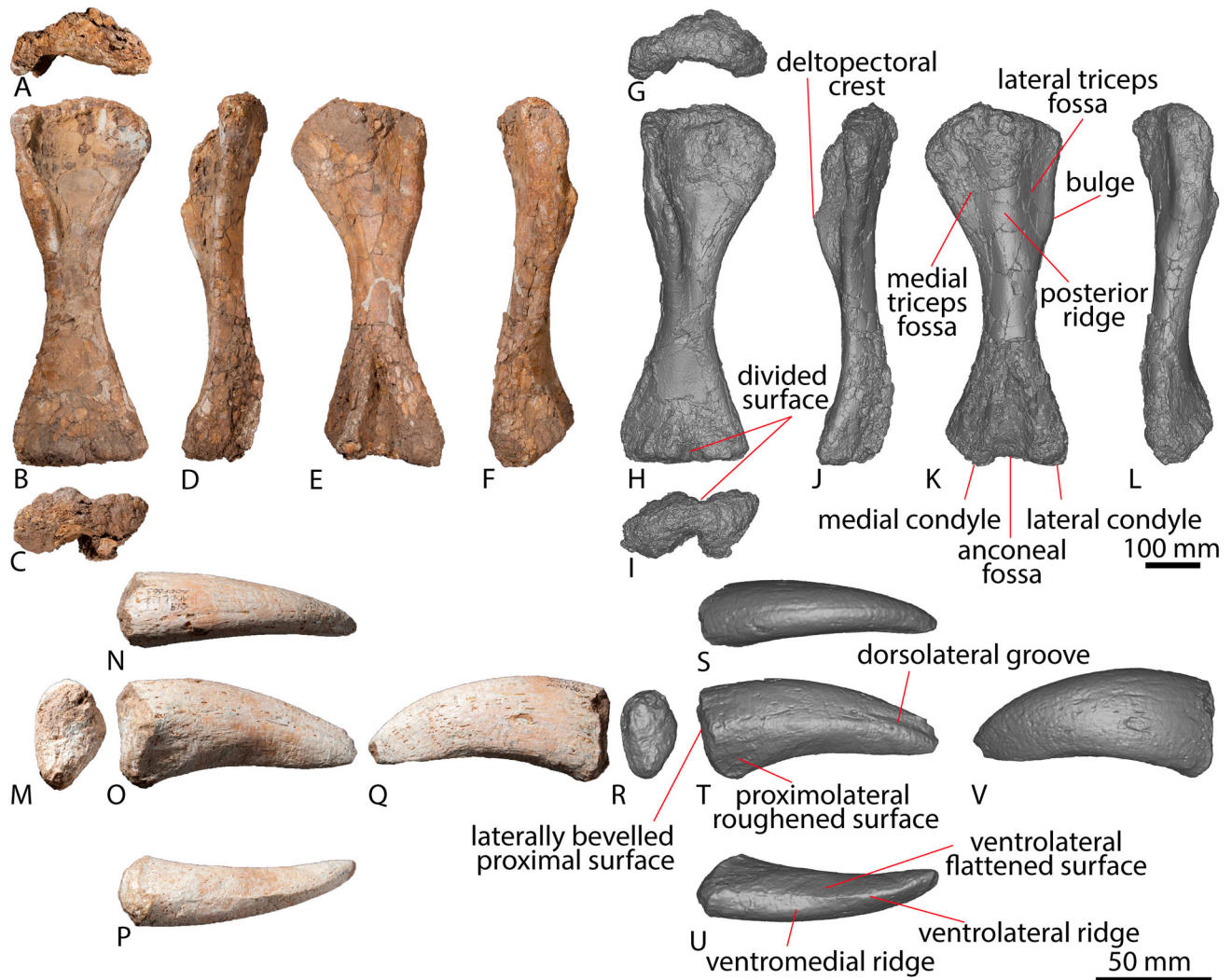


FIGURE 8. AODF 663 right humerus and right manual ungual. Right humerus photographs in **A**, dorsal, **B**, anterior, **C**, ventral, **D**, medial, **E**, posterior, **F**, lateral views. Right humerus digital models in **G**, dorsal, **H**, anterior, **I**, ventral, **J**, medial, **K**, posterior, **L**, lateral views. Right manual ungual in **M**, proximal, **N**, dorsal, **O**, anterior, **P**, ventral, **Q**, posterior views. Right manual ungual digital models in **R**, proximal, **S**, dorsal, **T**, anterior, **U**, ventral, and **V**, posterior views.

autapomorphic feature thereof by Poropat et al. (2015a), does not appear to be present in AODF 663.

Humerus

The right humerus of AODF 663 (Fig. 8A–L) is virtually complete. As a result of its close proximity to the ‘black soil’–siltstone interface, the posterior surface of the humerus has suffered some fragmentation, particularly the humeral head and the distal condyles. The humerus is hourglass-shaped, narrowing significantly mediolaterally at the midshaft. The proximal expansion is primarily along the medial margin, as is the case in most titanosauriforms (Poropat et al., 2016). The humeri of the named Winton Formation sauropod species appear more robust and do not narrow as significantly as that of AODF 663. When scaled to the same size, *Diamantinasaurus* and AODF 663 have an almost identical hourglass curvature along the medial proximodistal edge (Fig. 9C). Although *Australotitan* also appears to have an hourglass shape (Hocknull et al., 2021), the flattened

deltopectoral crest limits clear observation of the overall original shape prior to its collapse.

The Robusticity Index (RI) of this humerus varies along the element (Table 2), with the midshaft width markedly narrower than the proximal and distal widths, which are equidimensional. The RIs of the proximal and midshaft widths of AODF 663 are smaller than *Diamantinasaurus* and *Australotitan*, although the RIs of the distal widths of all three specimens are similar (Table 2). The RIs of *Wintonotitan* and *Savannasaurus* cannot be assessed as the humeri thereof are incomplete (Poropat et al., 2015a, 2020).

In proximal view, the anterior margin is concave and the posterior margin is convex. The proximal margin is very similar to that of *Diamantinasaurus* when scaled to the same size (Fig. 9C), and the anteroposterior thickness of the proximal end is greatest along the medial half of the element. The lateral margin, which comprises the deltopectoral crest, is markedly narrower, as in *Diamantinasaurus* (Poropat et al., 2015b). Proximally, the humeral head is less pronounced in AODF 663 than *Diamantinasaurus*, but this could be a result

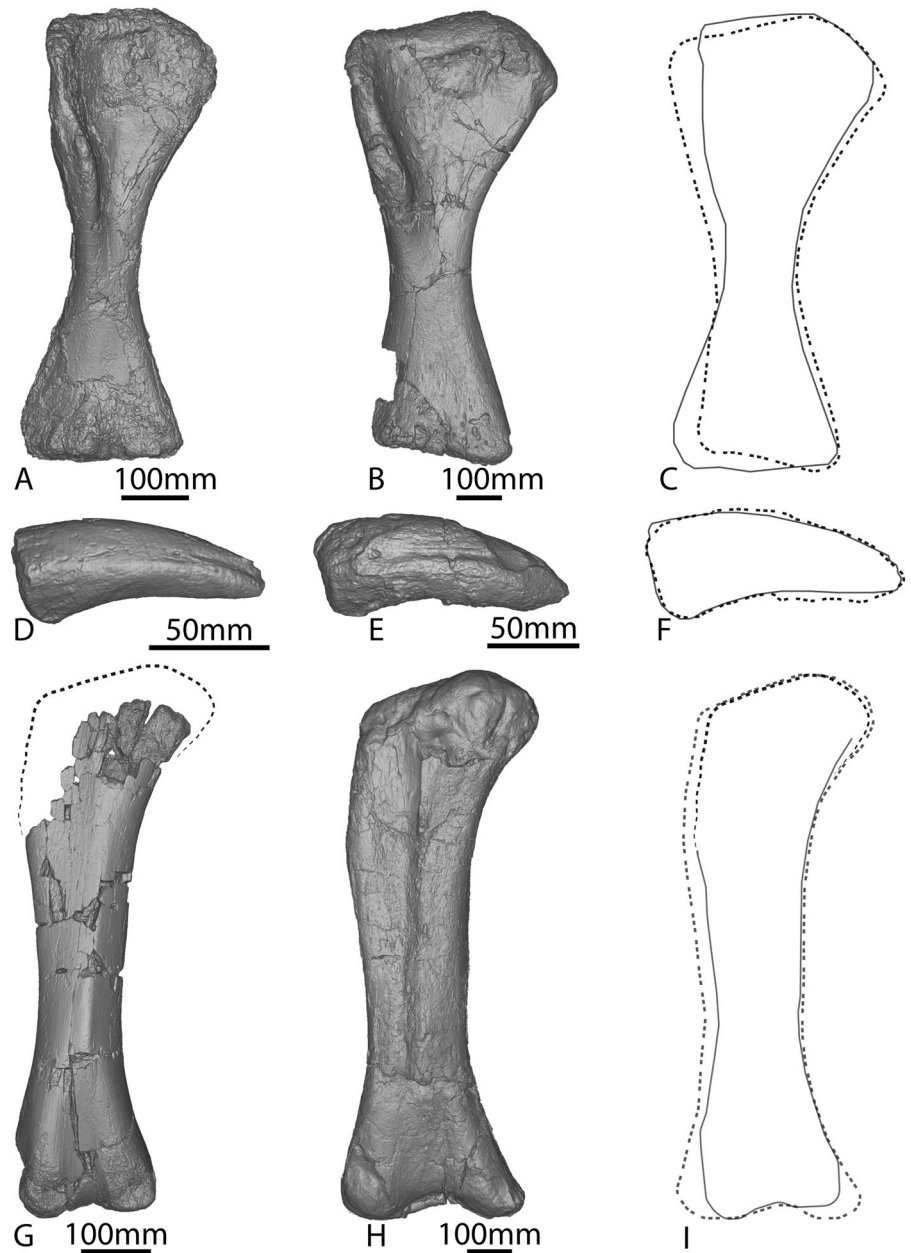


FIGURE 9. Comparisons between appendicular elements. **A**, AODF 663 right humerus in anterior view. **B**, AODF 603 left humerus mirrored in anterior view. **C**, AODF 663 (solid line) and AODF 603 (dotted line) humerus outlines overlaid to the same size. **D**, AODF 663 right manual ungual in anterior view. **E**, AODF 603 right manual ungual in anterior. **F**, AODF 663 (solid line) and AODF 603 (dotted line) manual ungual outlines overlaid to the same size. **G**, AODF 663 right femur with estimated proximal shape in anterior view. **H**, AODF 603 right femur in anterior view. **I**, AODF 663 (solid line) and AODF 603 (dotted line) femur outlines overlaid to the same size.

of taphonomic processes rather than a genuine point of difference.

The proximal half of the anterior surface is mediolaterally and proximodistally concave between the well-developed deltopectoral crest and the medial margin. Within the proximal fossa there is no tuberosity or distinct rugosity for the insertion site for *M. coracobrachialis*; however, given that this tuberosity is present in all neosauropods for which this can be assessed (Tschopp et al., 2015; Poropat et al., 2016; Mannion et al., 2019), its absence is likely to be ontogenetic. A distinct medial ridge, which autapomorphically characterizes the holotype of *Diamantinasaurus* (Poropat et al., 2015b), also does not appear to be present within the proximal fossa. Similarly, the small ridge observed in the anterior fossa of *Australotitan* by Hocknull et al. (2021) is not present on AODF 663.

The deltopectoral crest is prominent and well-developed, and projects exclusively anteriorly, as in *Diamantinasaurus* (Poropat et al., 2015b); this contrasts with the medial deflection of this feature observed in most somphospondylans (Wilson, 2002; Mannion et al., 2013). The deltopectoral crest extends distally to the humeral mid-length, as in the better-preserved humerus of *Diamantinasaurus* (Poropat et al., 2015b) and *Australotitan* (Hocknull et al., 2021), but unlike *Wintonotitan* (Poropat et al., 2015a) and *Savannasaurus* (Poropat et al., 2020), wherein the deltopectoral crest appears to terminate proximal to mid-length.

At its proximal end, the deltopectoral crest is mediolaterally narrow (36 mm), becoming broader at its mid-length (52 mm) and maintaining a similar breadth until fading out at the mid-shaft (Table S1). The distal portion of the deltopectoral crest is

TABLE 2. Humerus Robusticity Index (RI) of AODF 663, *Diamantinasaurus* (AODF 603), and *Australotitan* (EMF 102). Calculations for AODF 663 and AODF 603 taken from Supplementary Table 1. Calculations for EMF 102 taken from Hocknull et al. (2021: table 3).

	<i>Diamantinasaurus matildae</i> AODF 663	<i>Diamantinasaurus matildae</i> AODF 603	<i>Australotitan cooperensis</i> EMF 102
Overall RI	0.29	0.36	0.35
Proximal width RI	0.36	0.46	0.48
Midshaft width RI	0.14	0.22	0.22
Distal width RI	0.36	0.35	0.34

mediolaterally expanded as in *Diamantinasaurus* (Poropat et al., 2015b), but unlike *Wintonotitan* (Poropat et al., 2015a) and *Australotitan* (Hocknull et al., 2021). A lack of overlapping material prevents comparison of this morphology with *Savannasaurus* (Poropat et al., 2016, 2020). At the proximal end of the broadest section of the deltopectoral crest, a raised node is present; a similar feature is present on a partial sauropod humerus from near Blackall, Queensland (QM F311: Molnar, 2011), although not in the type specimen of *Diamantinasaurus* (Poropat et al., 2015b).

The proximal portion of the posterior surface is broadly mediolaterally convex, more so than *Wintonotitan* (Poropat et al., 2015a), *Savannasaurus* (Poropat et al., 2020), and *Australotitan* (Hocknull et al., 2021). A vertical central posterior ridge extends distally to the midshaft, as in *Diamantinasaurus* (Poropat et al., 2015b) and probably *Australotitan* (Hocknull et al., 2021). Either side of this broad ridge, a shallow, proximodistally elongate concavity is present, as in *Diamantinasaurus* (Poropat et al., 2015b) and *Wintonotitan* (Poropat et al., 2015a), but unlike *Australotitan* (Hocknull et al., 2021). This concavity does not appear to be present in *Savannasaurus* (Poropat et al., 2020). These subtly concave regions represent the sites of attachment of the humeral triceps (Klinkhamer et al., 2018b). A subtle bulge is present at the posterolateral margin, at approximately one-third of the shaft length; this coincides with the maximum development of the deltopectoral crest on the anterolateral margin and characterizes most titanosaurs (Upchurch et al., 2015), as well as *Wintonotitan* (Poropat et al., 2015a), but it appears to be absent in *Diamantinasaurus* (Poropat et al., 2015b) and *Australotitan* (Hocknull et al., 2021). The relevant region of the humerus of *Savannasaurus* is too incomplete to assess the presence or absence of this feature (Poropat et al., 2020). This bulge has been interpreted as the insertion site for either *M. scapulohumeralis anterior* or *M. deltoideus clavicularis* (Borsuk-Bialynicka, 1977; Upchurch et al., 2015; Otero, 2018).

The anterior surface of the humerus is essentially flat at midshaft, becoming shallowly mediolaterally convex along the distal third. At the mid-shaft, the posterior margin is mediolaterally convex, essentially representing an extension of the broadly mediolaterally convex region at the proximal end. This surface is maintained along the length of the shaft until the proximal margin of the anconeal fossa. At mid-length, the shaft is anteroposteriorly compressed, with a ‘D’-shaped cross section, as in *Diamantinasaurus* (Poropat et al., 2015b), but unlike the elliptical cross section of *Wintonotitan* (Poropat et al., 2015a) and bilobed sub-rectangular cross section of *Australotitan* (Hocknull et al., 2021). The subtle ridges separating the anterior and posterior surfaces of *Savannasaurus* (Poropat et al., 2020) are not present in AODF 663.

At the distal end, the medial half of the element is shallowly convex. Along the distal anterior margin, a distinct anterior bulge is present slightly lateral to the mid-line, separated from the medial half by a shallow concave region, and a second, less prominent bulge is present further laterally still. Collectively, these presumably represent a surface to which a cartilaginous cap would have adhered. The distal anterior surface is also divided in *Diamantinasaurus* (Poropat et al., 2015b), differing from nearly all other titanosaurs wherein the anterior surface of the lateral distal condyle is undivided (D’Emic, 2012).

Along the distal posterior margin, the anconeal fossa is deep and well-developed; this appears to have been partially exaggerated by the taphonomic processes of the ‘black soil.’ Both distal ridges (i.e., medial and lateral) have been fragmented and infiltrated, causing them to expand outwards and to appear more prominent. The bone within the anconeal fossa remains unaffected; the morphology of this bone demonstrates that the anconeal fossa was much deeper than any of the concavities on the anterior distal surface, but does not reveal the original depth of this feature. Nevertheless, the anconeal fossa is situated between the somewhat more strongly developed lateral condyle and the seemingly weaker (albeit possibly somewhat deformed) medial condyle. As preserved, both medial and lateral ridges appear to be deflected laterally; this might have been exaggerated by post mortem taphonomic processes, since the medial margin of the medial condyle appears to have suffered some minor crushing.

Manual Phalanx

The manual ungual phalanx of AODF 663 (Fig. 8M–V) is well preserved, with only a small amount of material missing from its proximal and distal ends. The identification of this element as a manual ungual is tentative, as it was not discovered in association with manual or pedal elements. However, its similarity with the preserved manual ungual of the *Diamantinasaurus* type individual (see Fig. 9F) leads us to favour this identification. It is interpreted as a right element since it is distinctly curved to the right in dorsal view, and its proximal surface is bevelled slightly laterally when considered as such (note that the type individual ungual was interpreted as a left element by Poropat et al. [2015b] but is reinterpreted here as a right manual phalanx I-2 based on comparisons with *Camarasaurus* [Tschopp et al., 2015]).

The ungual is proximodistally elongate, with a proximal height: proximodistal length ratio of 0.43, almost identical to the unusually low ratio of 0.40 that was proposed as a local autapomorphic feature for *Diamantinasaurus* (Poropat et al., 2015b). In proximal view, the ungual is essentially oval, with the ventral margin acutely convex. As preserved, the proximal surface is mediolaterally convex and slightly concave dorsoventrally; however, the incomplete preservation of this end might mean that this does not reflect the original morphology. The medial margin of the proximal end is very shallowly convex dorsoventrally, and the dorsal margin is broadly convex mediolaterally. Its lateral margin is somewhat pointed, formed by an essentially straight dorsolateral margin and a somewhat longer (but no less straight) ventrolateral margin that meet at ~120°, as also observed in *Diamantinasaurus* (Poropat et al., 2015b).

The medial surface of the ungual is dorsoventrally and proximodistally convex along its length, as in *Diamantinasaurus* (Poropat et al., 2015b). The transition between the medial and dorsal surfaces is smooth and indistinct. Ventrally, the medial surface terminates in a slight ridge. This ridge is only subtly expressed when compared with a second, more prominent ridge positioned further laterally. These ridges define a proximodistally concave, mediolaterally flat, and distally narrowing surface, which terminates at three-quarters the length of the phalanx. At this point, the more medial ventral ridge disappears, and the more lateral ridge becomes more pronounced.

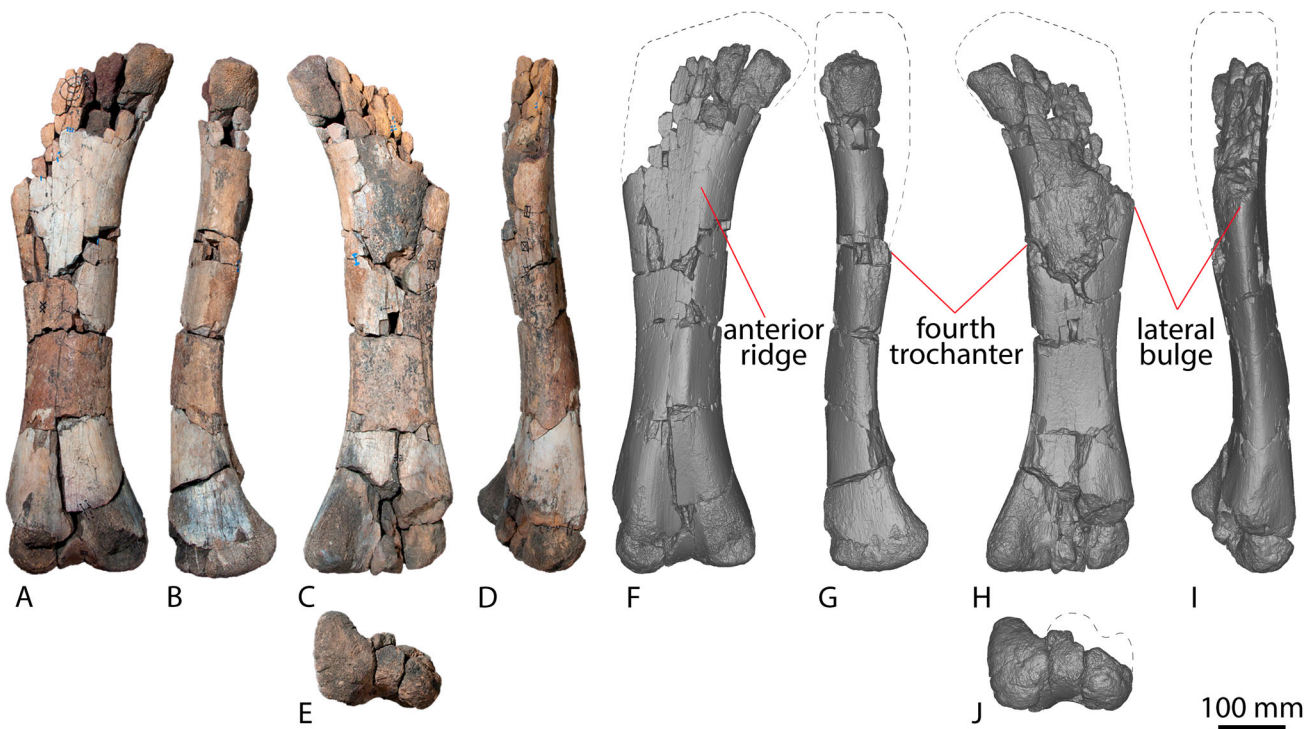


FIGURE 10. AODF 663 right femur. Photographs in **A**, anterior, **B**, medial, **C**, posterior, **D**, lateral, **E**, ventral views. Digital models in **F**, anterior, **G**, medial, **H**, posterior, **I**, lateral, and **J**, ventral views.

The lateral surface can be broadly separated into dorsolateral and ventrolateral sections; these are separated by a ridge that extends from the proximal junction of these two surfaces to the distal tip of the phalanx. Dorsal to this ridge, a subtle groove is present, most strongly expressed at the distal end. A similar lateral ridge and groove appear to be present in *Diamantinasaurus* (Poropat et al., 2015b), although they are pronounced more proximally than in AODF 663. Ventral to the ridge, the lateral surface is essentially flat dorsoventrally, but concave proximodistally, except at the proximal end where a flat, roughened patch is present. The distal tip of the ungual appears blunt, although this might have been exaggerated by incomplete preservation.

Femur

The right femur of AODF 663 (Fig. 10) was pieced together from fragments collected in the ‘black soil’ and is missing material from its proximal end, especially along the lateral margin, and the posterolateral portion of the distal end. Owing to the incomplete preservation of the proximal end, it is not possible to determine if a lateral trochanteric shelf was present; however, it is clear that a lateral bulge was present at approximately one-third of the length of the shaft, as in other titanosauriforms (Salgado et al., 1997).

The shaft of the femur is anteroposteriorly compressed (Table S1), similar to that of *Diamantinasaurus* (Fig. 9I) (Poropat et al., 2015b), but less so than in *Australotitan* (Hocknull et al., 2021). Along its length, the medial margin is more broadly curved than the more convex lateral margin; at the mid-length, therefore, the cross section of the femur is ovate and less compressed, with a flattened posterior margin and a shallowly convex anterior margin. The ratio of the mediolateral width to the antero-posterior length of the shaft is 1.74; this means that AODF 663 displays the plesiomorphic state for Sauropoda, i.e., a value less than 1.85 (Wilson, 2002), comparable with the ratio of 1.80 observed in

Diamantinasaurus (Poropat et al., 2015b), but significantly less than the ratio in *Australotitan* (>2.1; Hocknull et al., 2021).

The anterior surface of the femur is gently mediolaterally convex towards the lateral bulge, and essentially flat towards the medial surface. A weak crest nearer the medial than the lateral side descends almost two-thirds the length of the shaft from the level of the lateral bulge towards the fibular condyle, angled proximomedially/distolaterally. This crest is the linea intermuscularis cranialis and is also present in *Diamantinasaurus* (Poropat et al. [2015b], despite being incorrectly stated as absent by Hocknull et al. [2021]), *Australotitan* (Hocknull et al., 2021), *Saltasaurines* (Otero, 2010), *Alamosaurus* (D’Emic, 2012), and *Uberabatitan* (Silva Junior et al., 2019). This crest is not as distinct as the straight medial ridge running the length of the shaft in *Diamantinasaurus* (Poropat et al., 2015b; Klinkhamer et al., 2018a).

The fourth trochanter is located at the junction between the medial and posterior surfaces and is only very subtly expressed as a low ridge. Distal to the fourth trochanter, the posterior surface is smooth and flat, similar to *Australotitan* (Hocknull et al., 2021; although we note that this might be a result of taphonomic processes), but contrasting with the deep concavity present at the distal end of the femur of *Diamantinasaurus* (Poropat et al., 2015b). The posterior intercondylar fossa would have been deeper than its anterior counterpart, as shown by the morphology of the external bone preserved in both fossae. The presence or absence of a ridge linking the posterior ridges of the fibular condyle could not be determined in AODF 663; this feature was considered to be autapomorphic for *Diamantinasaurus* by Poropat et al. (2015b), and appears to also be present in *Australotitan* (Hocknull et al., 2021).

The distal condyles appear to be only weakly expressed on the anterior surface; however, both are incompletely preserved and worn, suggesting that they might have been more prominent in life. The distal margin is almost perpendicular relative to the long axis of the femur, differing from *Diamantinasaurus*,

wherein the fibular condyle extends further distally than the tibial condyle (Poropat et al., 2015b).

DISCUSSION

Taxonomic Assignment to *Diamantinasaurus matildae*

Detailed comparison with other Australian Cretaceous sauropods indicates that AODF 663 is most probably a specimen of *Diamantinasaurus matildae*. This is based on the shared presence of several previously recognized autapomorphies in the two published individuals (AODF 603 [holotype individual, including remains formerly regarded as paratypes (e.g., Poropat et al., 2015)] and AODF 836 [referred individual]) of *Diamantinasaurus*, as well as numerous differences with other taxa. Although several features that have been proposed as autapomorphies of *Diamantinasaurus* are absent in AODF 663, and thus could indicate that the latter specimen represents a different species, many of these features can potentially be attributed to the ontogenetic immaturity of the remains of the latter individual. Here, we discuss the presence or absence of these autapomorphic features in AODF 663.

Diamantinasaurus Ontogeny

The cervical rib of AODF 663 possesses the autapomorphic ridge of *Diamantinasaurus* and other defining longitudinal ridges. The ventral surfaces of the dorsal centra of AODF 663 are distinctly convex, in contrast to the concavity of osteologically mature *Diamantinasaurus* specimens; however, the vertebrae preserved in previously described *Diamantinasaurus* specimens mostly derive from the middle–posterior part of the dorsal series, meaning there may not be direct serial overlap with AODF 663. Furthermore, the ventral concavity is not as well defined in the middle dorsal vertebrae of AODF 836 as it is in the middle–posterior vertebrae of AODF 603. It is therefore possible that the morphology of the ventral surface differed with serial position in *Diamantinasaurus*, with a concavity absent in anterior dorsal vertebrae. Conversely, a concavity bound by ventral ridges might have developed through ontogeny to aid in muscle attachment and weight bearing. Some of the vertebral laminae and fossae of AODF 663 are also less defined than in AODF 663 and AODF 836. We interpret this as an increase in vertebral strength through ontogeny, as has also been proposed in the early diverging eusauropod *Shunosaurus lii* (Ma et al., 2021).

The scapular glenoid of AODF 663 is medially bevelled, which is the condition in nearly all members of Somphospondyli (Wilson, 2002), with the exception of the adult specimens of *Diamantinasaurus*, for which a laterally deflected scapular glenoid is a local autapomorphy (Poropat et al., 2015b, 2021). In addition, the scapula of AODF 663 lacks the distinct process on the ventral margin and accessory longitudinal ridge of osteologically mature specimens of *Diamantinasaurus*. These could have developed through ontogeny to aid in muscle attachment and weight-bearing purposes (as outlined in Klinkhamer et al., 2018b). In support of that interpretation, the defining autapomorphic ridges and fossae on the anterior surface of the proximal humerus of the *Diamantinasaurus* type specimen (see Klinkhamer et al., 2018b) appear to be faintly present in AODF 663 and thus potentially developed as the individual grew. The proximal humeri of both AODF 663 and AODF 603 possess a distinct central posterior ridge. Additionally, the lateral distal condyle of the humerus is divided in both specimens, which is a local autapomorphy of *Diamantinasaurus* within Titanosauria (D’Emic, 2012; Poropat et al., 2015b). A lateral ridge and groove are present on the manual ungual of both AODF 663 and AODF 603. The proximal height to proximodistal length ratio of the manual ungual of AODF 663 and AODF 603 are almost identical

(see Fig. 9F); this feature is locally autapomorphic for *Diamantinasaurus*. The femoral linea intermuscularis cranialis is present in the femur of both AODF 663 and AODF 603, with the only difference being that it is less defined in the former specimen. As the linea intermuscularis cranialis is a major point of muscle attachment in titanosaurian femora (Otero, 2010), it might have become more prominent as *Diamantinasaurus* grew.

AODF 663 is the smallest sauropod individual to be discovered in Australia. In life, it would have been approximately 4.2 metric tons in mass (calculated using the equations presented in Benson et al., 2014). When compared with the material of the osteologically mature *Diamantinasaurus matildae* holotype, dorsal vertebra B from AODF 663 is 55% the anteroposterior non-condylar centrum length of dorsal vertebra B from AODF 603, the scapula is 51% the proximodistal length, the humerus is 65% the proximodistal length, the manual ungual I-2 is 60% the proximodistal length, and the femur—despite being incomplete—is ~60% the proximodistal length of AODF 603. Overall, this puts AODF 663 at ~60% the size of AODF 603. The variability in proportional size shows that the bones of *Diamantinasaurus* did not grow isometrically, instead growing allometrically, as outlined in Table S2. These results indicate that the vertebrae and scapula of AODF 663 grew at a slower proportional rate than the humerus, manual ungual and femur, implying that the long bones were disproportionately larger than the rest of the body during early ontogeny.

The scapula of AODF 663 displays positive allometry in terms of proximodistal length when compared with AODF 603, whereas the humerus displays negative allometry (see Table S2). The long bones of AODF 663 (humerus and femur) are relatively narrower mediolaterally at the midshaft than those of AODF 603, displaying positive allometry (Fig. 9 and Table S2), and indicating—perhaps unsurprisingly—that the long bones of *Diamantinasaurus* became more proportionally robust through ontogeny. The humerus RIs (Table 2) of AODF 603 and AODF 663 indicate a lack of distal mediolateral expansion through ontogeny; rather, the proximal end and midshaft became more robust and ‘grew into’ the distal end. This is further evidenced by the proximal and mid-shaft mediolateral widths of the humerus of AODF 663 displaying positive allometry, and the distal humerus mediolateral width displaying negative allometry when compared with the humerus of AODF 603. Coupled with the ‘simplicity’ of the scapula of AODF 603, this might indicate that *Diamantinasaurus* required a relatively more robust shoulder joint as it grew, with the shoulder joint taking on the increase in weight-bearing tasks when compared with the less-robust elbow. The manual ungual of AODF 663 displays negative allometry in all its measured dimensions (see Table S3).

Owing to the incompleteness of dorsal vertebra B and the scapula of AODF 603 (see Fig. 3), it is difficult to ascertain the level of shape similarity between it and AODF 663; however, when scaled to the same size and overlapped, the completely preserved portions appear to be congruent (Fig. 3F, L). When scaled and compared with the complete scapula of an undescribed sauropod specimen from the Winton Formation (AODF 888), AODF 663 is virtually identical (Fig. 3J). Similarly, the manual unguals of AODF 603 and AODF 663 are virtually identical when scaled to the same size (Fig. 9F).

Overview of Ontogenetic Patterns in Sauropods

The vulcanodontid *Tazoudasaurus naimi* is the earliest-branching sauropod for which the ontogenetic growth pattern has been evaluated. This taxon shows isometric growth in the dorsal neural arch, ulna, ischium, tibia, and astragalus, but allometric growth in the humerus (Allain and Aquesbi, 2008). By contrast, the eusauropods *Patagosaurus fariasi* and *Shunosaurus*

lil both show only an allometric growth pattern. *Patagosaurus* has allometric growth in all assessed elements, including the teeth, coracoid, femur, and tibia (Bonaparte, 1986; Coria, 1994; Rauhut, 2003). *Shunosaurus* demonstrates allometry in the vertebrae, scapula, humerus, radius and fibula, and no major differences in the femur (Ma et al., 2021) (see Table S3 for further information). The phylogenetic affinities of the eusauropod *Bel-lusaurus sui* are uncertain and it is known only from juvenile material, but it has been hypothesized that the skull would have experienced allometric growth throughout ontogeny (Dong, 1990; Mo, 2013; Moore et al., 2018). Within Neosauropoda, diplodocoids present a range of ontogenetic growth patterns. Apatosaurine specimens display isometric growth in the humerus, femur, and pubis (Carpenter and McIntosh, 1994; Bonnan, 2004; Schwarz et al., 2007), with morphological consistencies observed throughout ontogeny in the vertebrae, scapula, and humerus (Forster, 2005). There is evidence of allometric growth in the tibia, with several character differences noted (Carpenter and McIntosh, 1994). Among diplodocines, isometric growth occurs in the shape of both the humerus and femur, and allometric growth occurs in the skull, vertebrae, and femoral proportions (see Table S3) (Curtice and Wilhite, 1996; Bonnan, 2004; Whitlock et al., 2010; Woodruff and Fowler, 2012; Tschopp and Mateus, 2013; Melstrom et al., 2016; Hanik et al., 2017; Woodruff et al., 2018).

Macronarians also exhibit substantial ontogenetic variability. The camarasauromorph *Europasaurus holgeri* demonstrates isometric growth in the ischium, and allometric growth in the skull, vertebrae, humeri, ulnae, and metacarpals (Sander et al., 2006; Carballido and Sander, 2014; Marpmann et al., 2015; Carballido et al., 2020). *Camarasaurus* specimens vary greatly, with isometry reported in the cranium, vertebrae, coracoid, the shape of the humerus and femur, and metatarsals, but allometry identified in the dentary, vertebrae, sternal plate, scapula, coracoid, proportions of the femur, and fibula (see Table S3) (Gilmore, 1925; Carpenter and McIntosh, 1994; Curtice and Wilhite, 1996; Bonnan, 2004; Forster, 2005; Ikejiri et al., 2005; Woodruff and Fowler, 2012). The brachiosaurid *Venenosaurus dicrocei* and several titanosaurs (including *Rinconsaurus caudamirus* and *Rapetosaurus krausei*) evidently grew isometrically, as observed in the ribs, ulnae, and manus of *Venenosaurus dicrocei* (Tidwell and Wilhite, 2005), all preserved elements of *Rinconsaurus caudamirus* (Calvo and González Riga, 2003), and the vertebrae, long bones, metacarpal III, pubis, tibia, fibula, and metatarsal I of *Rapetosaurus krausei* (Curry Rogers and Forster 2001, 2004; Curry Rogers et al., 2016; Curry Rogers and Kulik, 2018). Although isometry is the typically observed growth pattern in *Rapetosaurus*, it is possible that there is some allometric growth in the femur of this taxon (Curry Rogers and Forster 2001, 2004; Curry Rogers et al., 2016; Curry Rogers and Kulik, 2018). *Rapetosaurus* fits the pattern observed in the early branching somphospondylan *Phuwiangosaurus sirindhornae*, as well as the titanosaur *Alamosaurus sanjuanensis*: the former taxon exhibits isometry in the vertebrae and scapulocoracoid, and allometry in the humerus and femur (Martin, 1994; Martin et al., 1994, 1999; Klein et al., 2009), whereas the latter species displays isometry in the humeral shaft and ischium, but allometry in the ends of the humerus (Coulson, 1998; Lehman and Coulson, 2002; Tykoski and Fiorillo, 2017). However, *Rapetosaurus* contrasts with other titanosaurs for which only allometric growth has been proposed, as evinced by the teeth of *Lirainosaurus astibiae* (Díez Díaz et al., 2012), the tibia and dermal armor of *Saltasaurus loricatus* (Powell, 1992; D'Emic and Wilson, 2011), and the embryonic skulls of titanosaurs from Auca Mahuevo (Chiappe et al., 1998, 2005; Salgado et al., 2005; Garcia et al., 2010).

The above review demonstrates the relatively small number of sauropod taxa for which growth patterns have been assessed. This is reflective of the relatively low overall number of juvenile

sauropod fossils across the world (Table S3), as well as the fact that the identification of juvenile sauropod material to species level can be problematic: ontogenetic osteological changes sometimes preclude the assignment of juvenile specimens to taxa based on adult holotypes. Similarly, the growth patterns of a single sauropod species or population cannot be applied to more inclusive clades with abandon. Potentially ontogenetically variable autapomorphies can create contention when referring unidentified juvenile material to osteologically mature holotypes and for specimens growing allometrically (as in AODF 663); it is likely that the absence of these features is merely a consequence of their ontogenetic stage. This becomes less of an issue with ontogenetic age; by the time a sauropod individual is considered a subadult, it should possess all autapomorphies of the adult equivalent (Carballido and Sander, 2014; Mannion et al., 2021).

Ontogenetic osteological changes observed in numerous sauropod species have meant that the establishment of new species on the basis of juvenile specimens has proven to be problematic. One reason for this is that osteologically immature specimens often exhibit anatomical characters more aligned with their ancestral state, owing to the simplicity of their bones (Martin, 1994; Martin et al., 1994; Schwarz et al., 2007; Woodruff and Fowler, 2012; Carballido and Sander, 2014; Tschopp et al., 2015). For this reason, we acknowledge the possibility that a different taxonomic position for AODF 663 might be resolved in the future. For this to occur, more diagnostic material across a range of osteological growth stages for both *Diamantinasaurus* and other sauropod taxa will need to be discovered from the Winton Formation.

Implications for the Ontogenetic Growth Patterns of Titanosaurs

The growth pattern of *Diamantinasaurus* proposed here conflicts with the hypothesis that all titanosaurs grew isometrically (Curry Rogers et al., 2016; Silva Junior et al., 2017). Indeed, assigning an osteological growth pattern to a sauropod based solely on its phylogenetic position is not practicable (see Table S3). This means that when new juvenile specimens are found and examined, their osteological growth pattern should be determined on a case-by-case basis. Until the growth patterns of more juvenile titanosaurs are determined worldwide, we posit that the isometric growth hypothesis proposed for *Rapetosaurus* (Curry Rogers et al., 2016) cannot be extended to titanosaurs in general, nor to all elements in any given taxon. Rather, a majority of juvenile titanosaurs have been found to employ an allometric growth pattern (see Table S3), implying that this strategy was more successful for the group.

CONCLUSIONS

The first juvenile sauropod recovered from Australia (AODF 663) is assigned to *Diamantinasaurus matildae* based on several anatomical features. As the smallest sauropod skeleton yet discovered in Australia (Fig. S3), it provides insight into the allometric nature of the growth strategy in *Diamantinasaurus*, with the long bones growing at a faster rate than other appendicular elements and vertebrae, whilst also becoming increasingly robust throughout ontogeny. Although AODF 663 does not possess all autapomorphies of *Diamantinasaurus* for which it could potentially be appraised, this appears to reflect the ontogenetic immaturity of the specimen rather than taxonomic difference. It is expected that future discovery of additional sauropod material in Australia will not only strengthen the validity of *Diamantinasaurus* but also expand the knowledge on the known skeletal elements for the species. The referral of AODF 663 to *Diamantinasaurus* increases the known number of juvenile titanosaurs found worldwide and suggests that titanosaurs did not all employ an isometric growth strategy.

ACKNOWLEDGMENTS

The authors would like to thank: S. Muir and I. Muir (Elderslie Station) for informing AAOD of the discovery of the ‘Oliver’ site, and for allowing the 2012 dig at the site to take place; AAOD staff and volunteers who participated in the excavation and preparation of ‘Oliver’; D. O’Boyle for contributing to the purchase of an Artec Space Spider handheld laser scanner which was used to scan specimens in the AAOD collection for the purposes of description and comparison; S. Hocknull and K. Spring (QM) for facilitating access to *Wintonotitan watsi* material in their collection (to SLR, SFP, and PDM); S. Hocknull and the Eromanga Museum of Natural History for sharing 3D models of *Australotitan cooperensis* via MorphoSource; and two anonymous reviewers for their insightful comments that greatly improved this manuscript. PDM’s contribution was supported by grants from The Royal Society (UF160216 and RGF\EA\201037).

ORCID

Samantha L. Rigby  <http://orcid.org/0000-0002-7403-0910>
 Stephen F. Poropat  <http://orcid.org/0000-0002-4909-1666>
 Philip D. Mannion  <http://orcid.org/0000-0002-9361-6941>
 Adele H. Pentland  <http://orcid.org/0000-0003-4827-1996>

LITERATURE CITED

- Allain, R., and N. Aquesbi. 2008. Anatomy and phylogenetic relationships of *Tazoudasaurus naimi* (Dinosauria, Sauropoda) from the late Early Jurassic of Morocco. *Geodiversitas* 30:345–424.
- Benson, R. B. J., N. E. Campione, M. T. Carrano, P. D. Mannion, C. Sullivan, P. Upchurch, and D. C. Evans. 2014. Rates of dinosaur body mass evolution indicate 170 million years of sustained ecological innovation on the avian stem lineage. *PLOS Biology* 12: e1001853.
- Bonaparte, J. F. 1986. Les Dinosaurés (Carnosaurés, Allosauridés, Sauropodes, Cétiosauridés) du Jurassique Moyen de Cerro Cóndor (Chubut, Argentine) (2^e partie et fin). *Annales de Paléontologie (Vert.-Invert.)* 72:325–386.
- Bonaparte, J. F., and R. A. Coria. 1993. Un nuevo y gigantesco saurópodo titanosaurio de la Formación Río Limay (Albiano-Cenomaniano) de la Provincia del Neuquén, Argentina. *Ameghiniana* 30:271–282.
- Bonnan, M. F. 2004. Morphometric analysis of humerus and femur shape in Morrison sauropods: implications for functional morphology and paleobiology. *Paleobiology* 30: 444–470.
- Borsuk-Białynicka, M. 1977. A new camarasaurid sauropod *Opisthocoelicaudia skarzynskii* gen. n., sp. n. from the Upper Cretaceous of Mongolia. *Palaeontologia Polonica* 37:1–64.
- Calvo, J. O., and B. J. González Riga. 2003. *Rinconsaurus caudamirus* gen. et sp. nov., a new titanosaurid (Dinosauria, Sauropoda) from the Late Cretaceous of Patagonia, Argentina. *Revista Geologica de Chile* 30:333–353.
- Carballido, J. L., and M. P. Sander. 2014. Postcranial axial skeleton of *Europasaurus holgeri* (Dinosauria, Sauropoda) from the Upper Jurassic of Germany: implications for sauropod ontogeny and phylogenetic relationships of basal Macronaria. *Journal of Systematic Palaeontology* 3:335–387.
- Carballido, J. L., J. S. Marpmann, D. Schwarz-Wings, and B. Pabst. 2012. New information on a juvenile sauropod specimen from the Morrison Formation and the reassessment of its systematic position. *Palaeontology* 55:567–582.
- Carballido, J. L., O. W. M. Rauhut, D. Pol, and L. Salgado. 2011. Osteology and phylogenetic relationships of *Tehuelchesaurus benitezii* (Dinosauria, Sauropoda) from the Upper Jurassic of Patagonia. *Zoological Journal of the Linnean Society* 163:605–662.
- Carballido, J. L., M. Schneil, N. Knötschke, and P. M. Sander. 2020. The appendicular skeleton of the dwarf macronarian sauropod *Europasaurus holgeri* from the Late Jurassic of Germany and a re-evaluation of its systematic affinities. *Journal of Systematic Palaeontology* 18:739–781.
- Carpenter, K., and J. McIntosh. 1994. Upper Jurassic sauropod babies from the Morrison Formation; pp. 265–278 in K. Carpenter, K. Hirsch, and J. R. Horner (eds.), *Dinosaur eggs and babies*. Cambridge University Press, Cambridge.
- Chiappe, L. M., F. D. Jackson, R. A. Coria, and L. Dingus. 2005. Nesting titanosaurs from Auca Mahuevo and adjacent sites: understanding sauropod reproductive behavior and embryonic development; pp. 285–302 in K. A. Curry Rogers, and J. A. Wilson (eds.), *The Sauropods: Evolution and Paleobiology*. University of California Press, Berkeley.
- Chiappe, L. M., R. A. Coria, L. Dingus, F. D. Jackson, A. Chinsamy, and M. Fox. 1998. Sauropod dinosaur embryos from the Late Cretaceous of Patagonia. *Nature* 396:258–261.
- Cook, A. G., S. E. Bryan, and J. J. Draper. 2013. Post-orogenic Mesozoic basins and magmatism; pp. 515–575 in P. A. Jell (ed.), *Geology of Queensland*. Geological Survey of Queensland, Brisbane.
- Coombs, W. P., and R. E. Molnar. 1981. Sauropoda (Reptilia, Saurischia) from the Cretaceous of Queensland. *Memoirs of the Queensland Museum* 20:351–373.
- Coria, R. A. 1994. On a monospecific assemblage of sauropod dinosaurs from Patagonia: implications for gregarious behavior. *Gaia* 10:209–215.
- Coulson, A. B. 1998. Sedimentology and taphonomy of a juvenile Alamosaurus site in the Javelina Formation (Upper Cretaceous), Big Bend National Park, Texas. Unpublished M.S. Thesis, Texas Tech University.
- Currie, P. J. 2003. Allometric growth in tyrannosaurids (Dinosauria: Theropoda) from the Upper Cretaceous of North America and Asia. *Canadian Journal of Earth Sciences* 40:651–665.
- Curry Rogers, K. A., and C. A. Forster. 2001. The last of the dinosaur titans: a new sauropod from Madagascar. *Nature* 412:530–534.
- Curry Rogers, K. A., and C. A. Forster. 2004. The skull of *Rapetosaurus krausei* (Sauropoda: Titanosauria) from the Late Cretaceous of Madagascar. *Journal of Vertebrate Paleontology* 24:121–144.
- Curry Rogers, K. A., and Z. Kulik. 2018. Osteohistology of *Rapetosaurus krausei* (Sauropoda: Titanosauria) from the Upper Cretaceous of Madagascar. *Journal of Vertebrate Paleontology* e1493689.
- Curry Rogers, K. A., M. Whitney, M. D. D’Emic, and B. Bagley. 2016. Precocity in a tiny titanosaur from the Late Cretaceous of Madagascar. *Science* 352:450–454.
- Curtice, B. D., and D. R. Wilhite. 1996. A re-evaluation of the Dry Mesa Dinosaur Quarry sauropod fauna with a description of juvenile sauropod elements; pp. 325–338 in A. C. Huffman, W. R. Lund, and L. H. Godwin (eds.), *Geology and Resources of the Paradox Basin*. Utah Geological Association Guidebook, no. 25. Salt Lake City: Utah Geological Association.
- D’Emic, M. D. 2012. The early evolution of titanosauriform sauropod dinosaurs. *Zoological Journal of the Linnean Society* 166:624–671.
- D’Emic, M. D., and J. A. Wilson. 2011. New remains attributable to the holotype of the sauropod dinosaur *Neuquensaurus australis*, with implications for saltosaurine systematics. *Acta Palaeontologica Polonica* 56:61–73.
- Dettmann, M. E., R. E. Molnar, J. G. Douglas, D. Burger, C. Fielding, H. T. Clifford, J. Francis, P. Jell, T. Rich, M. Wade, P. V. Rich, N. Pledge, A. Kemp, and A. Rozefelds. 1992. Australian Cretaceous terrestrial faunas and floras: biostratigraphic and biogeographic implications. *Cretaceous Research* 13:207–262.
- Díez Díaz, V., X. Pereda Suberbiola, and J. L. Sanz. 2012. Juvenile and adult teeth of the titanosaurian dinosaur *Lirainosaurus* (Sauropoda) from the Late Cretaceous of Iberia. *Geobios* 45: 265–274.
- Dong, Z. 1990. Sauropoda from the Kelameili Region of the Junggar Basin, Xinjiang Autonomous Region. *Vertebrata Palasiatica*, 28:43–58.
- Fletcher, T. L., and S. W. Salisbury. 2014. Probable oribatid mite (Acari: Oribatida) tunnels and faecal pellets in silicified conifer wood from the Upper Cretaceous (Cenomanian-Turonian) portion of the Winton Formation, central-western Queensland, Australia. *Alcheringa* 38:541–545.
- Fletcher, T. L., P. T. Moss, and S. W. Salisbury. 2013. Foliar physiognomic climate estimates for the Late Cretaceous (Cenomanian-Turonian) Lark Quarry fossil flora, central-western Queensland, Australia. *Australian Journal of Botany* 61:575–582.
- Fletcher, T. L., P. T. Moss, and S. W. Salisbury. 2015. Wood growth indices as climate indicators from the Upper Cretaceous (Cenomanian-Turonian) portion of the Winton Formation, Australia. *Palaeogeography, Palaeoclimatology, Palaeoecology* 417:35–43.
- Fletcher, T. L., P. T. Moss, and S. W. Salisbury. 2018. The palaeoenvironment of the Upper Cretaceous (Cenomanian-Turonian) portion of the Winton Formation, Queensland, Australia. *PeerJ* 6:e5513.

- Forster, J. R. 2005. New juvenile sauropod material from Western Colorado, and the record of juvenile sauropods from the Upper Jurassic Morrison Formation; pp. 141–153 in V. Tidwell, and K. Carpenter (eds.), *Thunder-Lizards: The Sauropodomorph Dinosaurs*. Indiana University Press, Bloomington Indiana.
- García, R., L. R. A. Salgado, R. A. Coria, and L. M. Chiappe. 2010. Osteología embrionaria de saurópodos titanosauroides de Neuquén (Argentina): aspectos ontogenéticos y evolutivos. *Ameghiniana* 47:409–430.
- Gilmore, C. W. 1925. A nearly complete articulated skeleton of *Camarasaurus*, a saurischian dinosaur from Dinosaur National Monument. *Memoirs of the Carnegie Museum* 10:347–384.
- Griffin, C. T., M. R. Stocker, C. Colleary, C. M. Stefanic, E. J. Lessner, M. Riegler, K. Formoso, K. Koeller, and S. J. Nesbitt. 2021. Assessing ontogenetic maturity in extinct saurian reptiles. *Biological Reviews* 96:470–525.
- Hanik, G. M., M. C. Lamanna, and J. A. Whitlock. 2017. A juvenile specimen of *Barosaurus* Marsh, 1890 (Sauropoda: Diplodocidae) from the Upper Jurassic Morrison Formation of Dinosaur National Monument, Utah, USA. *Annals of Carnegie Museum* 84:253–263.
- Hocknull, S. A., M. Wilkins, R. A. Lawrence, V. Konstantinov, S. Mackenzie, and R. Mackenzie. 2021. A new giant sauropod, *Australotitan cooperensis* gen. et sp. nov., from the mid-Cretaceous of Australia. *PeerJ* 9:e11317.
- Hocknull, S. A., M. A. White, T. R. Tischler, A. G. Cook, N. D. Calleja, T. Sloan, and D. A. Elliott. 2009. New mid-Cretaceous (latest Albian) dinosaurs from Winton, Queensland, Australia. *PLoS ONE* 4:e6190.
- Hone, D. W. E., and O. W. M. Rauhut. 2010. Feeding behaviour and bone utilization by theropod dinosaurs. *Lethaia* 43:232–244.
- Hone, D. W. E., A. A. Farke, and M. J. Wedel. 2016. Ontogeny and the fossil record: what, if anything, is an adult dinosaur? *Biology Letters* 12:20150947.
- Ikejiri, T. 2015. Modes of ontogenetic allometric shifts in crocodylian vertebrae. *Biological Journal of the Linnean Society* 116:649–670.
- Ikejiri, T., V. Tidwell, and D. Trexler. 2005. New adult specimens of *Camarasaurus lentus* highlight ontogenetic variation within the species; pp. 154–179 in V. Tidwell, and K. Carpenter (eds.), *Thunder-Lizards: The Sauropodomorph Dinosaurs*. Indiana University Press, Bloomington, Indiana.
- Klein, N., and P. M. Sander. 2008. Ontogenetic stages in the long bone histology of sauropod dinosaurs. *Paleobiology* 34:247–263.
- Klein, N., M. Sander, and V. Suteethorn. 2009. Bone histology and its implications for the life history and growth of the Early Cretaceous titanosaur *Phuwiangosaurus sirindhornae*; pp. 217–228 in E. Buffetaut, G. Cuny, J. Le Loeuff, and V. Suteethorn. (eds.), *Late Palaeozoic and Mesozoic Ecosystems in SE Asia*. The Geological Society, London, Special Publications 315.
- Klinkhamer, A. J., H. Mallison, S. F. Poropat, G. H. K. Sinapius, and S. Wroe. 2018a. Three-dimensional musculoskeletal modelling of the sauropodomorph hind limb: the effect of postural change on muscle leverage. *Anatomical Record* 301:2145–2163.
- Klinkhamer, A. J., H. Mallison, S. F. Poropat, T. Sloan, and S. Wroe. 2018b. Comparative three-dimensional moment arm analysis of the sauropod forelimb: implications for the transition to a wide-gauge stance in titanosaurs. *Anatomical Record* 302:794–817.
- Kundrát, M., R. A. Coria, T. W. Manning, D. Snitting, L. M. Chiappe, J. Nudds, and P. E. Ahlberg. 2020. Specialized craniofacial anatomy of a titanosaurian embryo from Argentina. *Current Biology* 30:1–7.
- Lehman, T. M., and A. B. Coulson. 2002. A juvenile specimen of the sauropod dinosaur *Alamosaurus sanjuanensis* from the Upper Cretaceous of Big Bend National Park, Texas. *Journal of Paleontology* 76:156–172.
- Livingston, V. J., M. F. Bonnan, R. M. Elsey, J. L. Sandrik, and D. R. Wilhite. 2009. Differential limb scaling in the American alligator (*Alligator mississippiensis*) and its implications for archosaur locomotor evolution. *The Anatomical Record: Advances in Integrative Anatomy and Evolutionary Biology* 292:787–797.
- Longman, H. A. 1933. A new dinosaur from the Queensland Cretaceous. *Memoirs of the Queensland Museum* 10:131–144.
- Ma, Q., H. Dai, C. Tan, N. Li, P. Wang, X. Ren, L. Meng, Q. Zhao, G. Wei, and X. Xu. 2021. New *Shunosaurus* (Dinosauria: Sauropoda) material from the middle Jurassic lower Shaximiao Formation of Yunyang, Chongqing, China. *Historical Biology* DOI:10.1080/08912963.2021.1962852.
- Mannion, P. D., E. Tschopp, and J. A. Whitlock. 2021. Anatomy and systematics of the diplodocoid *Amphicoelias altus* supports high sauropod dinosaur diversity in the Upper Jurassic Morrison Formation of the USA. *Royal Society Open Science* 8:210377.
- Mannion, P. D., P. Upchurch, R. N. Barnes, and O. Mateus. 2013. Osteology of the Late Jurassic Portuguese sauropod dinosaur *Lusotitan atalaiensis* (Macronaria) and the evolutionary history of basal titanosauriforms. *Zoological Journal of the Linnean Society* 168:98–206.
- Mannion, P. D., P. Upchurch, D. Schwarz, and O. Wings. 2019. Taxonomic affinities of the putative titanosaurs from the Late Jurassic Tendaguru Formation of Tanzania: phylogenetic and biogeographic implications for eusauropod dinosaur evolution. *Zoological Journal of the Linnean Society* 20:1–126.
- Marpmann, J. S., J. L. Carballido, P. M. Sander, and N. Knötschke. 2015. Cranial anatomy of the Late Jurassic dwarf sauropod *Europasaurus holgeri* (Dinosauria, Camarasauromorpha): ontogenetic changes and size dimorphism. *Journal of Systematic Palaeontology* 13:221–263.
- Marsh, O. C. 1878. Principal characters of American Jurassic dinosaurs: Part I. *American Journal of Science* 16:411–416.
- Martin, V. 1994. Baby sauropods from the Sao Khua Formation (Lower Cretaceous) in Northeastern Thailand; pp. 147–154 in M. G. Lockley, V. F. Santos, C. A. Meyer, and A. P. Hunt (eds.), *Aspects of Sauropod Paleobiology* Gaia 10, Lisbon, Portugal.
- Martin, V., E. Buffetaut, and V. Suteethorn. 1994. A new genus of sauropod dinosaur from the Sao Khua Formation (Late Jurassic or Early Cretaceous) of northeastern Thailand. *Comptes Rendus, l'Academie des Sciences de Paris* 319:1085–1092.
- Martin, V., V. Suteethorn, and E. Buffetaut. 1999. Description of the type and referred material of *Phuwiangosaurus sirinhornae* Martin, Buffetaut and Suteethorn, 1994, a sauropod from the Lower Cretaceous of Thailand. *Oryctos* 2:39–91.
- Martínez, R. D. F., M. C. Lamanna, F. E. Novas, R. C. Ridgely, G. A. Casal, J. E. Martínez, J. R. Vita, and L. M. Witmer. 2016. A basal lithostrotian titanosaur (Dinosauria: Sauropoda) with a complete skull: implications for the evolution and paleobiology of Titanosauria. *PLoS ONE* 11:e0151661.
- Melstrom, K. M., M. D. D'Emic, D. Chure, and J. A. Wilson. 2016. A juvenile sauropod dinosaur from the Late Jurassic of Utah, U.S.A., presents further evidence of an avian style air-sac system. *Journal of Vertebrate Paleontology* 36:e1111898.
- Mo, J. 2013. *Topics in Chinese Dinosaur Paleontology: Bellusaurus sui*. Zhengzhou: Henan Science and Technology Press, 231.
- Molnar, R. E. 2011. New morphological information about Cretaceous sauropod dinosaurs from the Eromanga Basin, Queensland, Australia. *Alcheringa* 35:329–339.
- Molnar, R.E., and S. W. Salisbury. 2005. Observations on Cretaceous sauropods from Australia; pp. 454–465 in: V. Tidwell, and K. Carpenter (eds.), *Thunder-lizards: The Sauropodomorph Dinosaurs*. Indiana University Press, Bloomington, Indiana.
- Moore, A. J., J. Mo, J. M. Clark, and X. Xu. 2018. Cranial anatomy of *Bellusaurus sui* (Dinosauria: Eusauropoda) from the Middle-Late Jurassic Shishugou Formation of northwest China and a review of sauropod cranial ontogeny. *PeerJ* 6:e4881.
- Otero, A. 2010. The appendicular skeleton of *Neuquensaurus*, a Late Cretaceous saltosaurine sauropod from Patagonia, Argentina. *Acta Palaeontologica Polonica* 55:399–426.
- Otero, A. 2018. Forelimb musculature and osteological correlates in Sauropodomorpha (Dinosauria, Saurischia). *PLoS ONE* 13: e0198988.
- Poropat, S. F., M. Kundrát, P. D. Mannion, P. Upchurch, T. R. Tischler, and D. A. Elliott. 2021a. Second specimen of the Upper Cretaceous Australian sauropod dinosaur *Diamantinasaurus matildae* provides new anatomical information on the skull and neck of early titanosaurs. *Zoological Journal of the Linnean Society* 192:610–674.
- Poropat, S. F., P. D. Mannion, P. Upchurch, S. A. Hocknull, B. P. Kear, and D. A. Elliott. 2015a. Reassessment of the non-titanosaurian somphospondylan *Wintonotitan watti* (Dinosauria: Sauropoda: Titanosauriformes) from the mid-Cretaceous Winton Formation, Queensland, Australia. *Papers in Palaeontology* 1:59–106.
- Poropat, S. F., P. D. Mannion, P. Upchurch, T. R. Tischler, T. Sloan, G. H. K. Sinapius, J. A. Elliott, and D. A. Elliott. 2020. Osteology of the wide-hipped titanosaurian sauropod dinosaur *Savannasaurus elliottorum* from the Upper Cretaceous Winton

- Formation of Queensland, Australia. *Journal of Vertebrate Paleontology* e1786836.
- Poropat, S. F., P. Upchurch, P. D. Mannion, S. A. Hocknull, B. P. Kear, T. Sloan, G. H. K. Sinapius, and D. A. Elliott. 2015b. Revision of the sauropod dinosaur *Diamantinasaurus matildae* Hocknull et al. 2009 from the middle Cretaceous of Australia: implications for Gondwanan titanosauriform dispersal. *Gondwana Research* 27:995–1033.
- Poropat, S. F., M. A. White, T. Ziegler, A. H. Pentland, S. L. Rigby, R. J. Duncan, T. Sloan, and D. A. Elliott. 2021b. A diverse Late Cretaceous vertebrate tracksite from the Winton Formation of Queensland, Australia. *PeerJ* 9:e11544.
- Poropat, S. F., J. P. Nair, C. E. Syme, P. D. Mannion, P. Upchurch, S. A. Hocknull, A. G. Cook, T. R. Tischler, and T. Holland. 2017. Reappraisal of *Austrosaurus mckillopi* Longman, 1933 from the Allaru Mudstone of Queensland, Australia's first named Cretaceous sauropod dinosaur. *Alcheringa* 41:543–580.
- Poropat, S. F., P. D. Mannion, P. Upchurch, S. A. Hocknull, B. P. Kear, M. Kundrát, T. R. Tischler, T. Sloan, G. H. K. Sinapius, J. A. Elliott, and D. A. Elliott. 2016. New Australian sauropods shed light on Cretaceous dinosaur palaeobiogeography. *Scientific Reports* 6:34467.
- Powell, J. E. 1992. Osteología de *Saltasaurus loricatus* (Sauropoda–Titanosauridae) del Cretácico Superior del noroeste Argentino; pp. 165–230 in J. L. Sanz, and A. D. Buscalioni (eds.), *Los Dinosaurios y Su Entorno Biótico: Actas del Segundo Curso de Paleontología in Cuenca*. Instituto 'Juan de Valdés', Cuenca, Spain.
- Rauhut, O. W. M. 2003. A dentary of *Patagosaurus* (Sauropoda) from the Middle Jurassic of Patagonia. *Ameghiniana* 40:425–432.
- Salgado, L., R. A. Coria, and J. O. Calvo. 1997. Evolution of titanosaurid sauropods. I: Phylogenetic analysis based on the postcranial evidence. *Ameghiniana*, 34, 3–32.
- Salgado, L., R. A. Coria, and L. M. Chiappe. 2005. Osteology of the sauropod embryos from the Upper Cretaceous of Patagonia. *Acta Palaeontologica Polonica* 50:79–92.
- Sander, P. M., O. Mateus, T. Laven, and N. Knötschke. 2006. Bone histology indicates insular dwarfism in a new Late Jurassic sauropod dinosaur. *Nature* 441:739–741.
- Sander, P. M., N. Klein, E. Buffetaut, G. Cuny, V. Suteethorn, and J. Le Loeuff. 2004. Adaptive radiation in sauropod dinosaurs: bone histology indicates rapid evolution of giant body size through acceleration. *Organisms, Diversity and Evolution* 4:165–173.
- Sanz, J. L., J. E. Powell, J. L. Loeuff, R. Martínez, and X. P. Suberbiola. 1999. Sauropod remains from the Upper Cretaceous of Laño (Northcentral Spain). *Titanosaur phylogenetic relationships. Estudios del Museo de Ciencias Naturales de Álava* 14:235–255.
- Schwarz, D., T. Ikejiri, B. H. Breithaupt, P. M. Sander, and N. Klein. 2007. A nearly complete skeleton of an early juvenile diplodocid (Dinosauria: Sauropoda) from the Lower Morrison Formation (Late Jurassic) of north central Wyoming and its implications for early ontogeny and pneumaticity in sauropods. *Historical Biology* 19:225–253.
- Senior, B.R., A. Mond, and P. L. Harrison. 1978. *Geology of the Eromanga Basin*. Bureau of Mineral Resources, Geology and Geophysics Bulletin 167:1–102.
- Sereno, P. C., A. L. Beck, D. B. Dutheil, H. C. E. Larsson, G. H. Lyon, B. Moussa, R. W. Sadleir, C. A. Sidor, D. J. Varricchio, G. P. Wilson, and J. A. Wilson. 1999. Cretaceous sauropods from the Sahara and the uneven rate of skeletal evolution among dinosaurs. *Science* 286:1342–1347.
- Silva Junior, J. C. G., A. G. Martinelli, and L. C. B. Ribeiro. 2017. Description of a juvenile titanosaurian dinosaur from the Upper Cretaceous of Brazil. *Cretaceous Research* 76:19–27.
- Silva Junior, J. C. G., T. S. Marinho, A. G. Martinelli, and M. C. Langer. 2019. Osteology and systematics of *Uberabatitan ribeiroi* (Dinosauria: Sauropoda): a Late Cretaceous titanosaur from Minas Gerais, Brazil. *Zootaxa* 4577:401–438.
- Tidwell, V., and D. R. Wilhite. 2005. Ontogenetic variation and isometric growth in the forelimb of the Early Cretaceous sauropod *Venenosaurus*; pp. 1870–196 in V. Tidwell, and K. Carpenter (eds.), *Thunder-lizards: The Sauropodomorph Dinosaurs*. Indiana University Press, Bloomington, Indiana.
- Tschopp, E., and O. Mateus. 2013. The skull and neck of a new flagellicaudatan sauropod from the Morrison Formation and its implication for the evolution and ontogeny of diplodocid dinosaurs. *Journal of Systematic Palaeontology* 11:853–888.
- Tschopp, E., O. Mateus, and R. B. J. Benson. 2015. A specimen-level phylogenetic analysis and taxonomic revision of Diplodocidae (Dinosauria, Sauropoda). *PeerJ* 3:e857.
- Tucker, R.T., E. M. Roberts, V. Darlington, and S. W. Salisbury. 2017. Investigating the stratigraphy and palaeoenvironments for a suite of newly discovered mid-Cretaceous vertebrate fossil-localities in the Winton Formation, Queensland, Australia. *Sedimentary Geology* 358:210–229.
- Tucker, R.T., E. M. Roberts, Y. Hu, A. I. S. Kemp, and S. W. Salisbury. 2013. Detrital zircon age constraints for the Winton Formation, Queensland: contextualizing Australia's Late Cretaceous dinosaur faunas. *Gondwana Research* 24:767–779.
- Tykoski, R. S., and A. R. Fiorillo. 2017. An articulated cervical series of *Alamosaurus sanjuanensis* Gilmore, 1922 (Dinosauria, Sauropoda) from Texas: a new perspective on the relationships of North America's last giant sauropod. *Journal of Systematic Palaeontology* 15:339–364.
- Upchurch P., P. M. Barrett, and P. Dodson. 2004. Sauropoda; pp. 259–322 in D. B. Weishampel, P. Dodson, and H. Osmólska (eds.), *The Dinosauria: Second Edition*. Berkeley, University of California Press.
- Upchurch, P., P. D. Mannion, and M. P. Taylor. 2015. The anatomy and phylogenetic relationships of “*Pelorosaurus*” *becklesii* (Neosauropoda, Macronaria) from the Early Cretaceous of England. *PLoS ONE* 10:e0125819.
- Van Hinsbergen, D. J. J., L. V. de Groot, S. J. van Schaik, W. Spakman, P. K. Bijl, A. Sluijs, C. G. Langereis, and H. Brinkhuis. 2015. A paleo-latitude calculator for paleoclimate studies. *PLoS ONE* 10:e0126946.
- Varricchio, D. J. 2011. A distinct dinosaur life history? *Historical Biology* 23:91–107.
- Wedel, M. J. 2003. The evolution of vertebral pneumaticity in sauropod dinosaurs. *Journal of Vertebrate Paleontology* 23:344–357.
- Whitlock, J. A. 2011. A phylogenetic analysis of Diplodocoidea (Saurischia: Sauropoda). *Zoological Journal of the Linnean Society* 161:872–915.
- Whitlock, J. A., J. A. Wilson, and M. C. Lamanna. 2010. Description of a nearly complete juvenile skull of *Diplodocus* (Sauropoda: Diplodocoidea) from the Late Jurassic of North America. *Journal of Vertebrate Paleontology* 30:442–457.
- Wilson, J. A. 1999. A nomenclature for vertebral laminae in sauropods and other saurischian dinosaurs. *Journal of Vertebrate Paleontology* 19:639–653.
- Wilson, J. A. 2002. Sauropod dinosaur phylogeny: critique and cladistic analysis. *Zoological Journal of the Linnean Society* 136:217–276.
- Wilson, J. A. and M. T. Carrano. 1999. Titanosaurs and the origin of “wide-gauge” trackways: a biomechanical and systematic perspective on sauropod locomotion. *Paleobiology* 25:252–267.
- Wilson, J. A., and P. C. Sereno. 1998. Early evolution and higher-level phylogeny of sauropod dinosaurs. *Society of Vertebrate Paleontology Memoir* 5, *Journal of Vertebrate Paleontology* 18(2, Supplement), 68 pp.
- Wilson, J. A., M. D. D'Emic, T. Ikejiri, E. M. Moacdieh, and J. A. Whitlock. 2011. A nomenclature for vertebral fossae in sauropods and other saurischian dinosaurs. *PLoS ONE* 6:e17114.
- Woodruff, D. C., and D. Fowler. 2012. Ontogenetic influence on neural spine bifurcation in Diplodocoidea (Dinosauria: Sauropoda): A critical phylogenetic character. *Journal of Morphology* 273:754–764.
- Woodruff, D. C., T. D. Carr, G. W. Storrs, K. Waskow, J. B. Scannella, K. K. Nordin, and J. P. Wilson. 2018. The smallest diplodocid skull reveals cranial ontogeny and growth-related dietary changes in the largest dinosaurs. *Scientific Reports* 8:14341.
- You, H.-L., D.-Q. Li, L.-Q. Zhou, and Q. Ji. 2008. *Daxiatitan binglingi*: a giant sauropod dinosaur from the Early Cretaceous of China. *Gansu Geology* 17:1–10.
- Young, C. C. 1935. Dinosaurian remains from Mengyin, Shantung. *Bulletin of the Geological Society of China* 14:519–534.

Submitted October 12, 2021; revisions received December 21, 2021; accepted February 1, 2022.

Handling Editor: Amy Balanoff.